Surface Modification of Inorganic Materials by Fluorination Treatments

Christophe Cardinaud, Alain Tressaud

Surface Modification of Inorganic Materials by Fluorination Treatments

Christophe Cardinaud[a] and Alain Tressaud[b]

[a]Institut des Matériaux de Nantes (IMN-CNRS), 2, rue de la Houssinière, BP 3229, 44322 Nantes Cedex, France; [b]Institut de Chimie de la Matière Condensée de Bordeaux (ICMCB-CNRS), Avenue du Dr. Albert Schweitzer, 33608 Pessac Cedex, France

14.1 Introduction

The surface characteristics of materials dominate the performance of the final products in many applications. For instance the mechanical behavior of composite materials are strongly dependent on the nature of the fiber/matrix interface, the lubricant properties are influenced by surface tribological effects, the success of bio-implants is mostly determined by biocompatibility, etc.

Surface treatments by exposure to very reactive atmospheres show several advantages when compared to more conventional methods:

- the chemical modification is limited to surface only and does not perturb the bulk properties,
- reaction temperature is very low and avoid thermal degradation of the material,
- non-equilibrium reactions are possible.

The exceptional reactivity of fluorine and fluorinating atmospheres has been demonstrated by the synthesis of a wide variety of inorganic fluorine compounds. Surface fluorination has been proposed for modifying and/or protecting the surface of various materials such as polymers, metal surfaces, tissues, biomaterials, carbon-based compounds (graphite, carbon blacks, diamond), inorganic ceramics (superconducting oxides, pigments). Depending on the expected properties of the treated materials, the fluorination can be carried out in plasma-enhanced conditions, for instance in radiofrequency plasmas of CF_4, NF_3, SF_6, or in F_2 or fluorinating gases under atmospheric pressure. In particular processing of materials by plasma techniques is being increasingly used in various areas of production and manufacturing. Plasma chemistry takes place under non-equilibrium conditions. This allows chemical reaction to occur at temperatures that are considerably lower than for thermal reactions taking place at thermodynamic equilibrium.

This chapter is organised as follows. Part I describes the basic concepts of plasma physics and chemistry, and successively presents the important parameters defining a cold plasma, some diagnostic techniques for plasma processing, then elements of fluorine-based plasma chemistry are given and finally a tentative to describe mechanisms of plasma fluorination of inorganic materials is made. Most of the notions describing the plasma and the interaction with the surface have been inspired from the following reference books: Grill [1], Manos and Flamm [2], Auciello and Flamm [3], Chapman [4], Lieberman and Lichtenberg [5]. In Part II, examples of surface modification of various classes of materials are presented in plasma conditions, then in various fluorinating media. It should be noted that the modification of surface properties by processes involving polymers, i.e. modification of surface polymers by fluorinated plasmas, surface polymerisation and deposition of metals on fluoropolymers, will not be considered in the following since they have been extensively treated in others [131].

14.2 Part I: Basic concepts of fluorine-based low pressure plasmas*

14.2.1 What is a cold plasma?

The word "plasma" has been used for the first time in 1928 by Langmuir [6] to describe ionised gases. The popular terminology "fourth state of matter", often used to define the plasma state, refers to the energy of its constituents and truly applies when these are in thermodynamic equilibrium one with each other such as in stars or in interstellar medium. Plasmas used for materials processing are out of equilibrium. They are generated by electromagnetic excitation, and often also called "cold plasmas" or "low pressure plasmas". A cold plasma can be described as a weakly ionised medium, which contains positive and negative charges in equal concentration moving in random directions among dominant neutral species.

One important feature is that this quasi-neutral gas of charged and neutral particles is characterised by a collective behaviour. The positive charges are atoms, molecules, or fragments of molecules which have lost electrons. The negative charges are generally electrons, but also in electronegative gases (and F-containing molecules such as SF_6 and CF_4 are among these) molecules or fragments to which are attached one or more electrons. To be maintained, the plasma needs to be fed with energy which replaces by some charge-generation mechanism the loss of charged particles by recombination or diffusion.

The second important feature about cold plasmas is that almost all the energy absorbed from the external electric field is gained by the electrons as they are by far the lightest of the charged constituents. This energy transfer proceeds through ohmic heating and stochastic heating. On the other hand the only efficient way the electrons can transfer their energy to the molecules of the gas is under inelastic collisions. As a result, even if the energy of the charged carriers and the neutral species tends to average by various collision processes and interactions, the system

*A list of symbols and subscripts that appear in this Part is given at the end of the chapter.

remains out of equilibrium and each plasma constituent (electrons, ions, neutral species) is characterised by a different energy distribution.

14.2.2 Important plasma parameters

The properties of the plasma, and the way the plasma interacts with the wall of the container or with any surface immersed in it (such as a sample) are described by a number of important parameters. A short review of some parameters is given hereafter, and typical values are reported in Table 1. In a first order approximation, parameters in the volume of the plasma control the formation of the active species and the chemical reactions in the gas phase, parameters at the plasma surface boundary control how these species interact with the surface. As described below this description is far too simple, and an important feedback exists between the plasma-surface interaction and the gas phase chemistry.

14.2.2.1 Parameters in the plasma volume

Densities and degree of ionisation. The neutral gas can be considered as in equilibrium with its container and described by the kinetic theory of gases. The neutral

Table 1

Typical range values for plasma parameters in rf diode and high density reactors, (calculation is done for a CF_4 plasma assuming Maxwell–Boltzmann distributions)

Plasma parameters (unity)	Rf diode (low density)	High density
P, pressure (Pa)	2.7–66.6	0.3–6.7
n_e, electronic density (m^{-3})	10^{16}–10^{15}	10^{18}–10^{16}
T_e, electron temperature (V)	5–8	3–5
n_n, neutral density (m^{-3})	$5\ 10^{20}$–$2\ 10^{22}$	$5\ 10^{19}$–$2\ 10^{21}$
α, degree of ionisation	10^{-5}–$5\ 10^{-8}$	10^{-2}–$5\ 10^{-6}$
λ_D, Debye length (m)	$2\ 10^{-4}$–$5\ 10^{-4}$	10^{-5}–$2\ 10^{-4}$
υ_{pe}, electron frequency (Hz)	10^9–$2\ 10^8$	10^{10}–10^9
υ_{pi}, ion frequency (Hz)	$2\ 10^6$–$5\ 10^5$	$2\ 10^7$–$2\ 10^6$
$\lambda_{e/n}$, e^-/n mean free path (m) (elastic) [88]	10^{-2}–$2\ 10^{-4}$	$2\ 10^{-1}$–$2\ 10^{-3}$
$\upsilon_{e/n}$, e^-/n coll. frequency (s^{-1}) (elastic) [88]	$2\ 10^9$–10^{10}	$5\ 10^6$–$5\ 10^9$
$\lambda_{n/n}$, n/n mean free path (m) (hard sphere)	$5\ 10^{-3}$–$2\ 10^{-4}$	$5\ 10^{-2}$–$2\ 10^{-3}$
$\upsilon_{n/n}$, n/n coll. frequency (s^{-1}) (hard sphere)	$5\ 10^4$–$2\ 10^6$	$5\ 10^4$–$2\ 10^5$
$\lambda_{i/n}$, i/n mean free path (m) (in sheath–polarisation)	$5\ 10^{-3}$–$2\ 10^{-4}$	$5\ 10^{-2}$–$2\ 10^{-3}$
$\upsilon_{i/n}$, i/n coll. frequency (s^{-1}) (in sheath–polarisation)	$5\ 10^5$–10^8	$5\ 10^4$–10^6
Φ_i, Bohm ion flux ($m^{-2}\ s^{-1}$)	$6\ 10^{19}$–$6\ 10^{18}$	$4\ 10^{21}$–$4\ 10^{19}$
s, average sheath thickness (m)	$2\ 10^{-3}$–10^{-2}	$5\ 10^{-4}$–$5\ 10^{-3}$

density n_n is thus related to the pressure P and temperature T by the Avogadro relation. The electron density n_e, also called the plasma density, is the number of electron per volume unit. In electropositive plasmas, ions are positive charges and ion density n_i equals electron density, otherwise neutrality says that $n_i^+ = n_i^- + n_e$. The degree of ionisation α is given by the fraction of molecules which are ionised:

$$\alpha = \frac{n_i}{n_n + n_i}.$$

Energy distributions. Since the plasma density is generally low, the energy distribution of neutral species $f(E_n)$ is essentially controlled by the random collision processes among themselves and with the wall of the container. Then $f(E_n)$ follows a Maxwell–Boltzmann distribution (MBD), and the average energy for the neutral particles is: $\langle E_n \rangle = \frac{3}{2} \cdot k \cdot T_n$ with $T_n \sim T_{\text{wall}}$. However in a real case each neutral species population may or may not be in equilibrium with one another depending on the various generation and loss processes taking place. The electrons gain energy through acceleration by the electric field. This energy is spent in the plasma along two processes [5]. In the plasma volume, electrons accelerated by local fields (ohmic heating), loose their energy through momentum transfer with thermal electrons and in inelastic collisions with neutral species, and a random distribution is obtained. Stochastic heating occurs in the sheaths by the reflection of the electrons on the oscillating sheath edge (an image is that of the reflection of a ball on a moving wall). The latter is the main mode of energy transfer in low-pressure plasmas. Very little change occurs in the electron energy distribution function $f(E_e)$ by elastic collisions between electrons and heavy particles, as the kinetic energy transfer varies as:

$$\frac{m_e \cdot m_p}{(m_e + m_p)^2}.$$

The fraction of electrons which gain enough energy to induce excitation, ionisation or dissociation processes with the neutral species loose all or part of their energy through inelastic collisions. Therefore $f(E_e)$ varies from one plasma to another according to the nature of the gas and the various inelastic processes taking place. As the bulk of the plasma is quasi-neutral, instantaneous and time averaged fields are weak, and the assumption of an MBD shape for $f(E_e)$ is generally reasonable. In the plasma jargon the electron mean energy $\langle E_e \rangle$ is expressed in eV and using the relation $\langle E_e \rangle = \frac{3}{2} \cdot k \cdot T_e$, an "equivalent electron temperature" in eV corresponding to the product $k \cdot T_e$ is generally used. As an example, an MBD for 3 eV electrons is compared in Fig. 1 to the experimental $f(E_e)$ for a high density CHF_3 plasma obtained from Langmuir probe measurements. In reactive gases, the high energy part of the distribution may be depleted due to inelastic collisions with the neutral species, and $f(E_e)$ can differ significantly from an MBD. However considering reaction rates, only the fraction of the electron population above the reaction threshold is concerned. Then estimation of the rate is possible whenever this fraction behaves as an MBD.

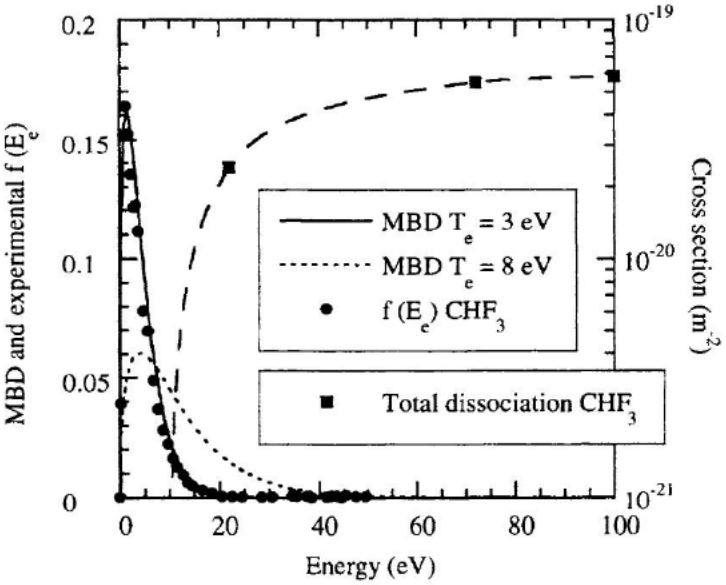

Fig. 1. Maxwell–Boltzmann electron energy distribution for 3 and 8 eV electrons, compared to experimental data for $f(E_e)$ in CHF_3. Also shown is the total dissociation cross section of CHF_3 (reproduced with permission from Phys. Rev., A25 (1982) 1420 [7]).

Debye length and plasma frequencies. The Debye shielding is another important feature of the collective behaviour of a plasma. Debye shielding is the response of the charged particles to reduce the effect of local electric fields. The electrons are more mobile because they are lighter, and thus they react more rapidly than the ions to this perturbation. So, any local excess of positive or negative charged particles creates an electric field which induces a collective response from the electrons to cancel this field. Assuming an MBD, the electric field reduces as

$$\exp\left[-\frac{r}{\lambda_D}\right],$$

with

$$\lambda_D = \sqrt{\frac{\varepsilon_0 \cdot k \cdot T_e}{e^2 \cdot n_e}}$$

the Debye length. The Debye length expresses the characteristic dimension of regions in which breakdown of charge neutrality can occur in a plasma. λ_D increases with decreasing n_e, so there is a low electron density limit for a ionised gas to be considered as a plasma, typically when λ_D is of the same order as the dimension of the discharge. This also means that the plasma cannot penetrate in parts or volumes of the process

chamber which have linear dimensions smaller than λ_D. Another important feature is that the Debye shielding is not complete. At a distance where the electrostatic potential is lower than $(k \cdot T_e/e)$ the charges can escape the charge cloud.

The response of the electrons to a potential perturbation induces oscillations of the electron cloud with a frequency

$$\upsilon_{pe} = \frac{1}{2 \cdot \pi} \sqrt{\frac{e^2 \cdot n_e}{m_e \cdot \varepsilon_0}}.$$

The product $\omega_{pe} \cdot \lambda_D \approx \langle c_e \rangle$ indicates that the electrons are able to respond sufficiently fast to maintain the plasma neutrality if a perturbation of angular frequency $\omega < \omega_{pe}$ is occurring. Similarly, an ion plasma frequency can be defined:

$$\upsilon_{pi} = \frac{1}{2 \cdot \pi} \sqrt{\frac{e^2 \cdot n_i}{m_i \cdot \varepsilon_0}}.$$

In rf driven plasmas at $\upsilon_{rf} = 13.56$ MHz, υ_{pi} is usually below υ_{rf} (except for very dense plasmas), whereas υ_{pe} is well above. A simple picture of the plasma with respect to the excitation field is that of a fast electron cloud moving in a sea of static ions.

The charged particle collective behaviour (and thus the plasma) exists only if random collision processes do not smear out the coherence of the motion of the charged particles. This means in practice that the frequency of the electron-neutral collisions has to remain smaller than the electron plasma frequency.

Collision frequencies, mean free paths, and cross sections. Collision processes are central to the description of chemical reactions in the plasma. The mean free path $\lambda_{A/B}$ of particle A is the mean distance this particle travels before encountering particle B. $\lambda_{A/B}$ is related to the mean velocity of particle A and to the mean collision frequency between A and B.

In the case of neutral species at thermal equilibrium ($\langle c_A \rangle \approx \langle c_B \rangle$), the hard sphere approximation leads to

$$\lambda_{A/B} = \frac{1}{\sqrt{2}} \cdot \frac{1}{n_B \cdot \pi \cdot (r_A + r_B)^2}.$$

With respect to plasma chemistry, the most important collision processes in a weakly ionised plasma occur between charged particles and neutral particles. Elastic collisions concern principally coulombic and polarisation scattering processes. Coulombic scattering applies when the characteristic interaction time

$$\left(\approx \frac{2 \cdot a_0}{c_{A/B}} \right)$$

is shorter than the characteristic electron orbital time scale ($\sim 10^{-17}$–10^{-16} s). So it concerns particles with $c_A > 10^6$ m s^{-1}, that is fast electrons, which are very few

in the plasma. On the contrary, when the characteristic interaction time is greater than 10^{-17} s, the neutral particle has time enough to polarise. With respect to the $c_{A/B}$ condition, polarisation scattering concerns ion-neutral collisions and low energy electron-neutral collisions. For electrons of low energies, this simple picture is often complicated by quantum mechanical effects (Ramsauer minimum effect) and in some cases the cross section shows no dependency with a velocity just as in the hard sphere approximation.

Inelastic collisions between electrons and atoms or molecules are of particular interest as they lead to excitation and ionisation states, which often induce dissociation of the molecule or enhance chemical reactivity. The general behaviour for electron energy of the electron-atom or molecule dissociative excitation or ionisation cross section is given by:

$$\sigma_{e/n}^{\text{exc,ion}}(E_e) = \pi \cdot \left(\frac{e^2}{4 \cdot \pi \cdot \varepsilon_0}\right)^2 \cdot \frac{1}{E_e} \cdot \left(\frac{1}{E_{\text{th}}} - \frac{1}{U}\right),$$

for $E_e > E_{\text{th}}$ and with E_{th} the threshold energy for the process, and U the limit for the energy transfer in the process (that is $U = \min(E_e, E_{\text{ith}})$ for excitation and $U = E_e$ for ionisation).

Dissociative electron attachment collisions are important in electronegative gases, and the corresponding cross section has the following general shape:

$$\sigma_{e/n}^{\text{att}}(E_e) \propto \pi \cdot \left(\frac{e^2}{4 \cdot \pi \cdot \varepsilon_0}\right)^2 \cdot \frac{E_e - E_{\text{th}}}{E_{\text{th}}^3},$$

for $E_{\text{th}} < E < E_{\text{th}} + \Delta E$.

Reaction rates. For electron-neutral reactions such as dissociation: $AB + e \rightarrow A + B + e$, the reaction rates are generally of the second order and have the general expression:

$$\frac{dn_{AB}}{dt} = K_{e/AB} \cdot n_e \cdot n_{AB},$$

with

$$K_{e/AB} = \int_0^\infty c_{e/AB} \cdot \sigma_{e/AB}^{\text{diss}} \cdot f(c_{e/AB}) \cdot dc_{e/AB}$$

the rate constant.

Figure 1 also shows an MBD for 8 eV electrons and the typical variation with energy of the total electron impact dissociation cross section for CHF_3 [7]. This points out that the fraction of the electron population which has enough energy to initiate gas phase chemistry is extremely dependent upon T_e.

14.2.2.2 Parameters at the plasma-surface boundaries

Sheaths, Bohm criterion and floating potential. Sheaths are regions of positive space charge which are formed at the boundary of the plasma with any surface in contact with it. The plasma is quasi-neutral, so charged particles are not confined and easily lost to the wall. Electrons which have much higher thermal velocities than ions reach an immersed surface faster. This creates a negative potential at the surface which repels the electrons towards the plasma, and induces a positive space charge around the surface where $n_e < n_i$ (Fig. 2). The Debye shielding effect limits the extension of the sheath in the plasma to few λ_D.

Assuming an MBD for the electrons, conservation of energy and flux for the ions (no collisions) through the sheath leads to a condition known as the Bohm criterion for the energy with which the ions enter the sheath:

$$E_i > \frac{k \cdot T_e}{2}.$$

This criterion means that the ions enter the sheath with a velocity much greater than their thermal velocity, and only depending on the electron temperature. The ions are thus accelerated by a weak electric field in a pre-sheath region in which the charge neutrality exists ($n_e = n_i$) as it is part of the plasma (Fig. 2). If one neglects the ion initial energy, the voltage drop across this region with respect to the plasma

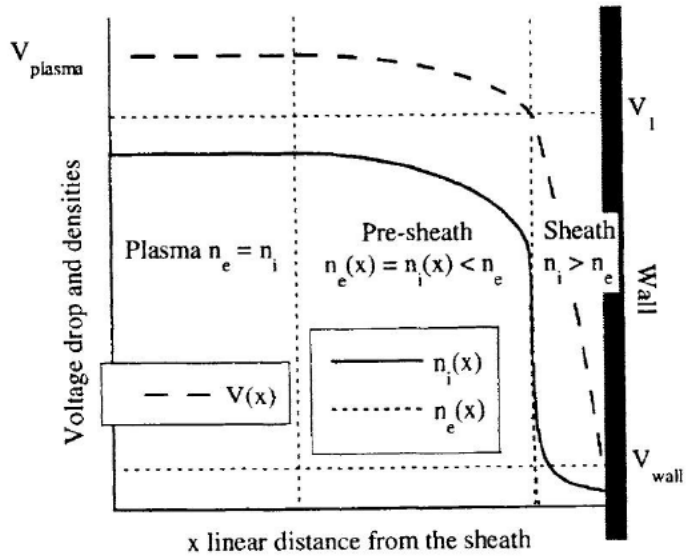

Fig. 2. Qualitative behaviour of the potential, and electron and ion densities drop in the sheath.

potential (V_p) is expressed by

$$V_l - V_p = -\frac{k \cdot T_e}{2 \cdot e}$$

(Fig. 2). The plasma potential depends on the electron temperature, it will thus vary from one gas to another as a function of the ionisation threshold of the gas: the lower E_{ith}, the greater the electron fraction to be able to ionise the gas, and thus at equilibrium the lower T_e and V_p.

In the case of a floating surface, equilibrium corresponds to the situation where the ion and electron fluxes are equal at the surface, then

$$\Phi_e = \Phi_i = n_e \cdot \sqrt{\frac{k \cdot T_e}{m_i}} \cdot \exp\left[-\frac{1}{2}\right]$$

and the voltage drop across the sheath is

$$V_f - V_l = \frac{k \cdot T_e}{2 \cdot e} \cdot \ln\left[2 \cdot \pi \cdot \frac{m_e}{m_i}\right]$$

(Fig. 2). As an important consequence, any surface immersed in the plasma is subjected during plasma processing to a positive ion bombardment.

As this ion assistance in the gas-surface chemistry may greatly influence the result of the plasma treatment, control of the ion flux and of the ion energy is a very important parameter in plasma processing. From the previous relation and the values of Table 1, one sees that the voltage drop across a floating sheath is typically 10–30 V. For processing purposes, it is often desirable to increase this bias and thus the ion energy. The most commonly encountered way to achieve this goal is to bias the surface under rf excitation as it allows processing of any materials: conductors, semiconductors, or insulators. In electronegative gases, formation of negative ions by electron attachment decreases the electron density, and replaces a fast and light negative charge by a slow and heavy one. This changes the properties of the sheath. The general trend is that the slow negative ions are more easily repelled into the plasma than the electrons would have been; this effect increases the importance of the electrons in the sheath, and reduces the voltage drop across the sheath. Negative ions which scarcely reach the surface are thus usually ignored in plasma-surface reaction schemes, but their indirect effect through the modification of the sheath characteristics may be important.

Ion flux and energy at a rf biased surface. In the most common experimental set-up this biased surface is insulated from the generator by a blocking capacitor. In rf diode reactors this electrode is also the one which excites the plasma; in rf triode plasma systems or in high density plasma reactors biasing allows to control the ion bombardment on the surface to be processed. In the presence of a blocking capacitor a situation very similar to the floating surface occurs. No current can

flow from the electrode to the external circuit, and the electrode is alternatively charged negatively and positively during an rf cycle. Due to the higher electron mobility, an average negative charge loads the electrode and equilibrium is obtained when ion and electron currents are cancelled on an average rf cycle. The voltage drop through the sheath is thus modulated along the rf cycle around a dc potential (V_{dc}) which is negative with respect to the plasma. The sheath thickness follows a similar rf modulation. Yet the general assumptions made in the previous section are still valid, and the time averaged ion flux on the surface is again given by the Bohm criterion:

$$\langle \Phi_i \rangle = n_e \cdot \sqrt{\frac{k \cdot T_e}{m_i}} \cdot \exp\left[-\frac{1}{2}\right]$$

So the ion flux on the surface is directly proportional to the plasma density.

The sheaths between the conductive plasma and the walls behave like capacitors, so a relation exists between the sheath voltages and the electrode areas A:

$$\frac{\langle V_p \rangle - V_{dc}}{\langle V_p \rangle} = \left[\frac{A_{\text{ground electrode}}}{A_{\text{rf electrode}}}\right]^n,$$

with $n \approx 1$ to 2.

The time taken by the ions to cross the sheath has a strong influence on their energy distribution when reaching the surface. If the ion average transit time is much longer than the rf period, then the ions feel only the average sheath voltage drop, whatever the instantaneous sheath potential when they enter the sheath. Their energy distribution is narrow and centred on $e \cdot (\langle V_p \rangle - V_{dc})$, this case is expected when $\upsilon_{pi} < \upsilon_{rf}$ and for collision-less sheaths. In the other case ($\upsilon_{pi} \gg \upsilon_{rf}$), the ion energy depends upon the instantaneous sheath potential at the moment the ion enter the sheath and the distribution can spread from the minimum to the maximum of the sheath voltage, that is between and $\langle V_f \rangle$ and $2 \cdot (\langle V_p \rangle - V_{dc}) - \langle V_f \rangle$. Figure 3 reports a very clear interpretation of the shape of the ion energy distribution at the driven electrode in a low-pressure CF_4 plasma [8]. These results are in excellent agreement with theory which predicts a broadening of the distribution proportional to $\sqrt{m_i}$ [9]. Although the excitation frequency is larger than the ion plasma frequency, the ions follow partially the rf modulated field in the sheath. The common approximation that the ions are "frozen" and "see" only the average sheath voltage is practical to estimate the average ion energy but actually applies only for heavy ions and in the case of collision-less sheaths.

Effect of pressure: collisions in the sheath. The values reported in Table 1 suggest that the collision-less sheath is a weak approximation. In normal operating pressures, ion-neutral collisions occur in the sheath ($\lambda_{i/n} <$ average sheath thickness). One can expect the average ion energy to decrease when increasing the pressure, and the ion energy distribution to be severely affected. The general trend given in Fig. 4 for the average ion energy on the grounded electrode [10] can be scaled on the

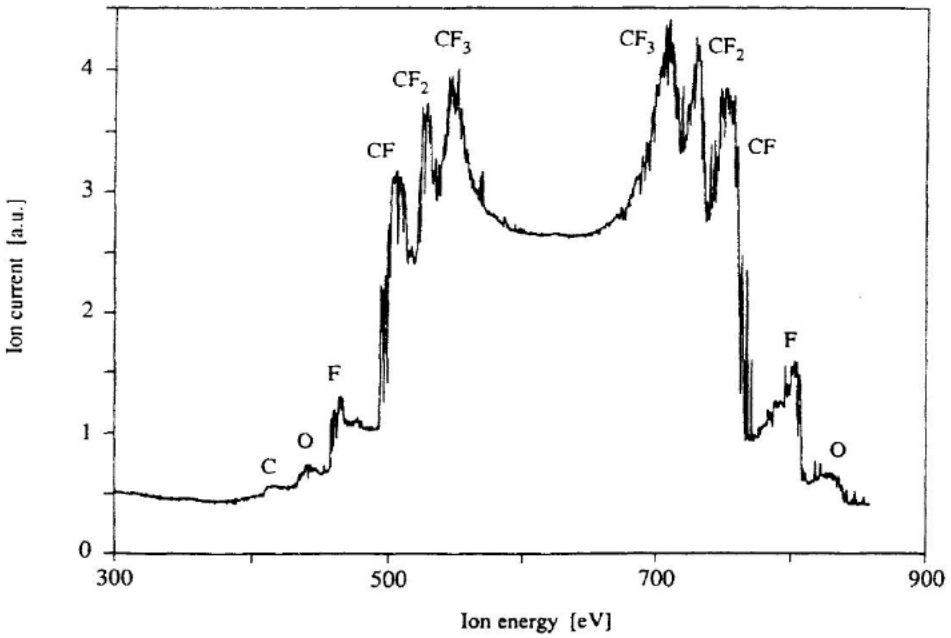

Fig. 3. Measured ion energy distribution in 3 mTorr CF_4 plasma (reprinted with permission from J. Appl. Phys., 67 (1990) 1229 [8])..

powered electrode. Charge exchange reactions, in which the ion becomes an energetic neutral and a thermal ion is created, and elastic scattering are the most probable processes for energy loss.

Figure 5 reports ion energy distributions at a rf-driven electrode in Cl_2 and SF_6-He plasmas as a function of operating pressure [11]. In both cases the energy distribution is broadened on the low energy side when the pressure is increased. For Cl_2 the distribution spreads over a wide energy range at $P > 10$ Pa with low energy structures due to charge exchange collisions (just as in Ar) In the case of SF_6/He, a large broadening is observed but no low energy features are present, possibly because of the occurrence of several ions in SF_6 plasmas [12]. Another important effect of collisions in the sheath is to random the direction of the ion velocities with respect to the surface (Fig. 4). Ions created via charge exchange processes have small incident angles, whereas ions suffering elastic collisions have a larger angle distribution.

14.2.3 Diagnostic techniques for plasma processing

The combination of analyses of both the plasma and the surface is probably the best strategy to improve the understanding of the plasma-surface interaction. A brief description of the most common techniques is given hereafter. Examples of applications are given here and later in Secs 14.2.4 and 14.2.5.

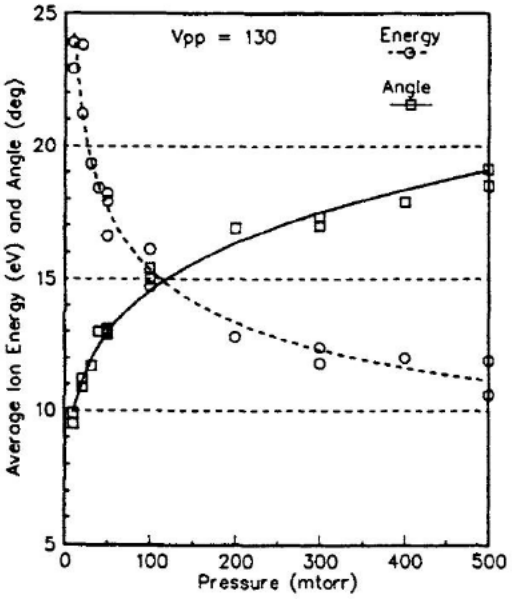

Fig. 4. Average ion energy and angle as a function of pressure (reprinted with permission from J. Appl. Phys., 68 (1990) 3916 [10]).).

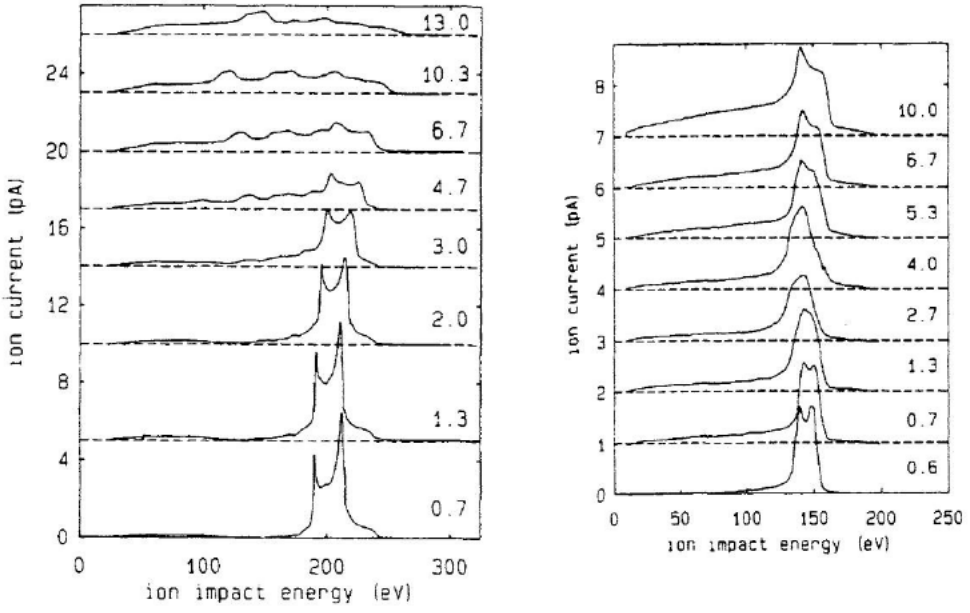

Fig. 5. Measured ion energy distribution in function of pressure (Pa), in Cl_2 (left) and SF_6—He (right) plasmas (reprinted with permission from J. Appl. Phys., 69 (1990) 1253 [11]).

14.2.3.1 Plasma diagnostics

Mass spectrometry. This technique is very attractive for in situ characterisation of plasma processing, as it can in principle detect all charged and neutral species. Sampling the plasma is achieved through a small orifice in the plasma reactor wall, the most efficient set-up are those where the extraction hood of the spectrometer itself is placed at the plasma boundary. The size of orifice should be less than λ_D so that the plasma does not get through. It should have an ideally "zero length" which means in practice that its length has to be shorter than $\lambda_{A/B}$ to minimise collision between the particles during their transport. In addition to the mass filter, modern mass spectrometers are frequently equipped with an energy analyser, which enables to obtain energy distributions of the plasma ions. Mass spectrometry has proven to be one of the most powerful techniques for the understanding of plasma processing. Reference data for inorganic fluorides gases can be found in Beattie [13]. If identification of gas phase molecular products is quite straightforward, as formation of C_xF_y ($x > 2$) species in C_2F_6 plasmas [14], detection of radicals or negative ions is less easy. Identification [15–17] and quantification [16] of radicals by the ionisation threshold method is possible. Figure 6 presents the intensity of CF_2^+ ions

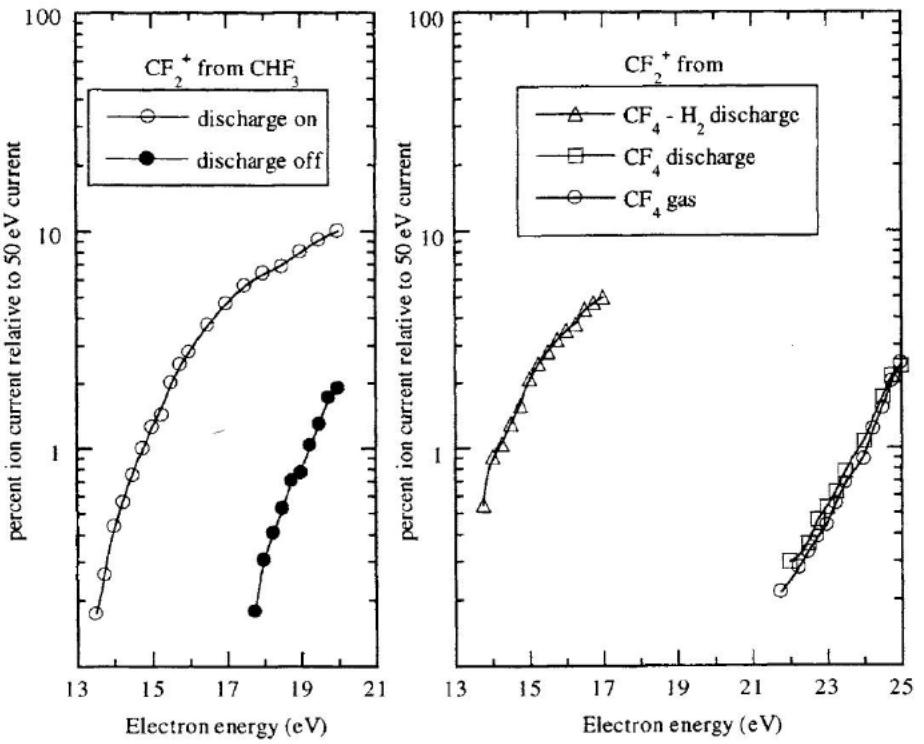

Fig. 6. Intensity of CF_2^+ as a function of electron energy in CHF_3, CF_4 and CF_4-H_2 plasmas (reprinted with permission from J. Appl. Phys. 50 (1979) 6594 [15]).

formed in the mass spectrometer ionisation chamber from direct ionisation or dissociative ionisation of neutral species vs the electron energy for CHF_3, CF_4 and CF_4-H_2 plasmas. Knowing the ionisation potential of CF_2 (11.8 V), and the dissociative ionisation potential of CHF_3 (14.7 V) and CF_4 (21 V) into CF_2^+, the results of Fig. 6 point out the presence of CF_2 radicals in CHF_3 and CF_4-H_2 plasmas and their absence in CF_4. Detailed reactions discussing the formation of CF_2 in CF_4 upon addition of H_2 to CF_4 are presented in Sec. 15.2.4. Recently "polymerisation" reactions in fluorocarbon plasmas have been investigated by using an electron dissociative attachment technique [18], and have shown the formation of C_nF_{2n-k} molecules up to $n=9$.

Negative ions are expected to be in large concentration in fluorinated molecules discharges. These ions are generally confined in the discharge as very few of them have enough energy to cross the sheaths. Detection of negative ions can be achieved through modulation of the discharge at low frequency [19]: since the sheath vanishes immediately as the plasma is cut off, the negative ions are able to reach the orifice of the mass spectrometer during the "plasma off" period. An alternative method uses photodetachment processes [20].

An important feature of mass spectrometry is the detection of volatile plasma-surface interaction products. Figure 7 reports the evolution of the production rate of WF_6 and WOF_4 from a tungsten surface in SF_6—O_2 plasma upon plasma exposure time [21]. At a first glance, the rather surprising feature in these results is that during the surface oxide elimination the dominant product is WF_6

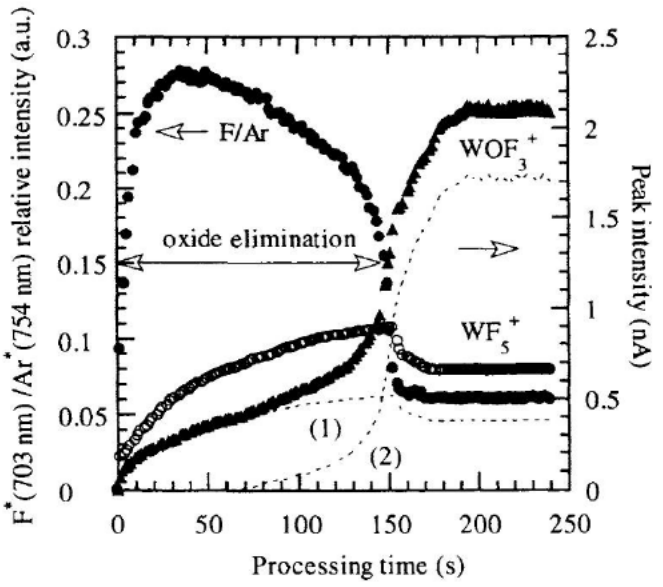

Fig. 7. Evolution of F/Ar, WF_5^+, and WOF_3^+ with time during processing of tungsten in SF_6—O_2 (reprinted with permission from J. Electrochem. Soc., 140 (1993) 505 [21]).

and not WOF_4, whereas the situation is reversed once the oxide is removed. The fluorination mechanism of W is discussed in Sec. 14.2.5.

Optical spectroscopies. These techniques are the least intrusive in situ plasma diagnostic methods. The most commonly used techniques are emission spectroscopy, absorption spectroscopy, laser-induced fluorescence.

Emission spectroscopy is the most popular since it is easy to implement. It is frequently used in industrial equipment for real-time control of a process. Very fine qualitative information of the plasma composition can be obtained. The drawback of this technique is that it provides information from excited species. These are only a small fraction of the total number of species, and they may be produced by more than one excitation pathway. Indeed the measured intensity I_{A^*} emitted by electron-excited species A^* from the ground state A can be expressed as:

$$I_{A*} = C(\lambda) \cdot g(A^*, \lambda) \cdot n_A \cdot n_e \cdot \int_{E_{th}}^{\infty} \sigma_{e/A}^{exc}(E_e) \cdot f(E_e) \cdot \sqrt{2 \cdot \frac{E_e}{m_e}} \cdot dE_e$$

with $g(A^*, \lambda)$ the emission probability of radiation λ from A^*, and $C(\lambda)$ the apparatus response. As a result it is extremely difficult and usually impossible to correlate the measured intensity to the absolute concentration of the parent ground state species A. Yet in fluorine plasmas, emission spectroscopy combined with actinometry technique [21–24] allows to measure relative variations of the atomic fluorine concentration in the plasma, as a function of time, space, or experimental conditions. Examples are given in Secs 14.2.4 and 14.2.5. When the actinometry rules are not fully verified, the general trend in the evolution of emitting plasma species (and their ground state parents) can still be investigated through intensity normalisation to a reference line, which eliminates the dependency of I_{A^*} with electron density.

Absorption spectroscopy and laser induced fluorescence (LIF), give access to the concentration of molecules, atoms, and ions in the ground state. LIF is enable to achieve highly spatial and time resolved analyses. This technique is thus particularly suitable to investigate composition changes in the plasma, and obtain spatial or time concentration profiles. Published results in fluorine plasmas using absorption [25–27] and LIF [28–32] mainly concern temperature measurements [25] or the quantification of CF_x radicals [26–31] in fluorocarbon-based plasmas and SO_x in SF_6—O_2 discharges [32]. Recently LIF has been used to measure plasma-surface interaction products [33].

Langmuir probes. Electrostatic probe measurements give access in principle to n_e, n_i, $\langle V_p \rangle$, T_e, and to the electron energy distribution. If the implementation is easy (collection of the current using a biased conductor), it is much more difficult to obtain reliable measurements because the method is very intrusive. Most of the probes have a cylindrical geometry, but some probes are planar or spherical. The following conditions have to be fulfilled preferably. Ideally the probe dimension has to be smaller than λ_D, to limit perturbation of the plasma, also the sheath thickness around the probe has to stay smaller than $\lambda_{i/n}$ or $\lambda_{e/n}$ in order to limit

collisions [34]. These conditions are difficult to fulfil and thus the plasma is generally less dense around the probe. Another critical problem arises from the surface of collection: as it theoretically includes the sheath around the probe, the surface of collection may not be precisely defined. Moreover it varies with the probe bias and oscillates with the rf modulation of the plasma [35]. A way to correct the probe from the rf oscillation is to give it an oscillating reference, either using an external bias at the same frequency as the rf excitation (active correction), or using the plasma itself via a capacitor (passive correction) [36]. Although difficult to obtain, probe characterisation of a plasma is a nice complementary diagnostic to optical emission. As an example, Fig. 8 compares Ar (used as an actinometer) emission intensity I_{Ar^*} (750.4 nm) in a CHF_3-based plasma with calculation of

$$K_{e/Ar} \cdot n_e = n_e \cdot \int_{E_{th}}^{\infty} \sigma_{e/Ar}^{exc}(E_e) \cdot f(E_e) \cdot \sqrt{2 \cdot \frac{E_e}{m_e}} \cdot dE_e$$

deduced from Langmuir probe measurements.

14.2.3.2 Surface diagnostics

Surface diagnostics gives fine complementary information to plasma diagnostics, providing that the surface can be analysed in situ and possibly in real-time, or in a such a way that it does not suffer any dramatic chemical or structural modifications.

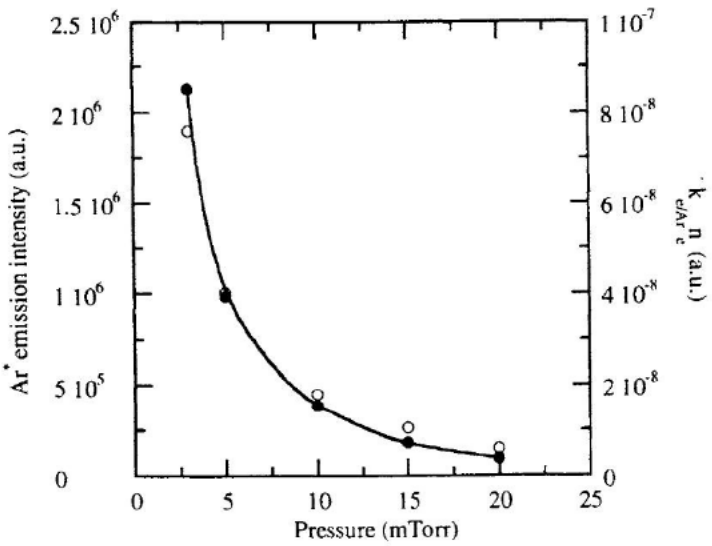

Fig. 8. Ar^* optical emission intensity compared to $K_{e/Ar} \cdot n_e$ from Langmuir probe measurements as a function of pressure, the Ar^* intensity being corrected for the variation of pressure.

X-ray photoelectron spectroscopy is probably the most commonly employed technique, as it gives information about the chemical species located in the first 15 nm below the surface. It is of particular interest if a vacuum transfer facility, from the processing chamber to the XPS, enables to avoid atmospheric contamination, as shown in Fig. 9. This experiment concerns W exposure to a SF_6 plasma. A sample transferred under vacuum is free of oxygen and carbon contamination as compared to a sample exposed to air between processing and analysis. In addition, the comparison of the surface chemistry in both cases gives some information on the nature of the chemical species. S is present on the W surface in the form of W–S species as in WS_2 compounds; these species are insensitive

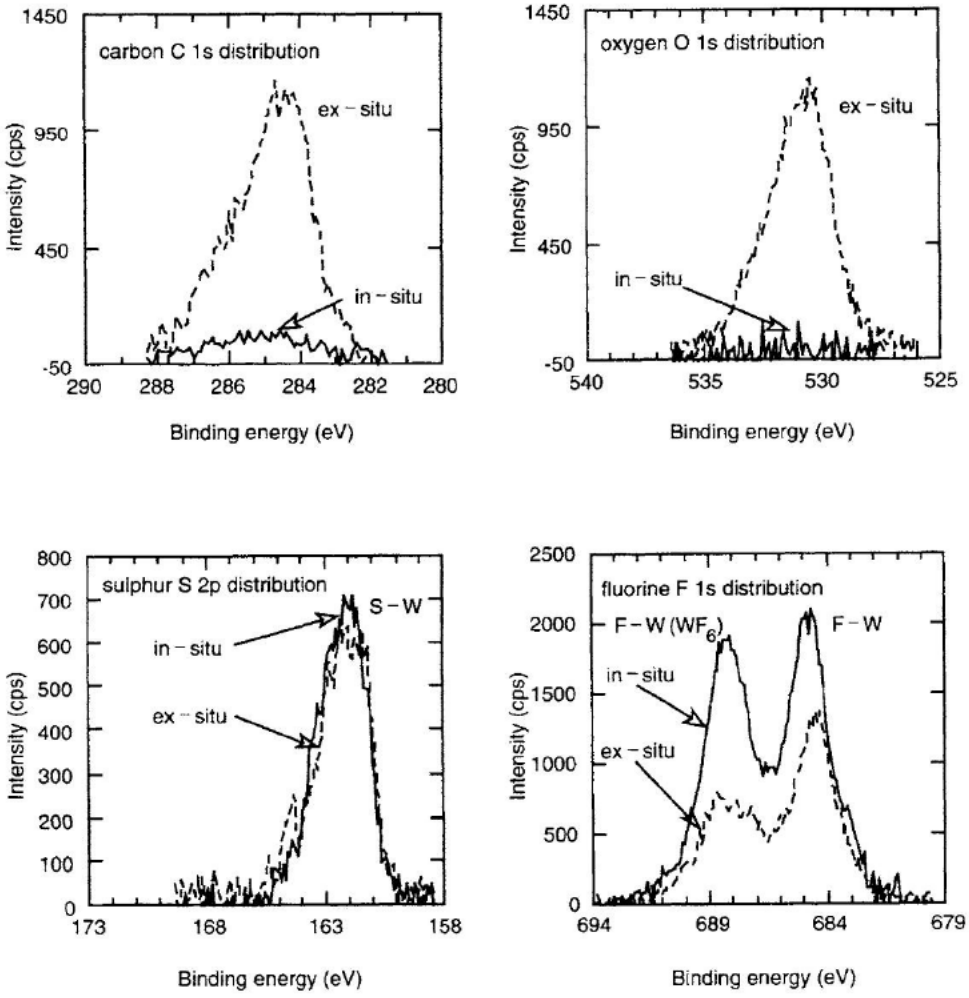

Fig. 9. XPS analysis of a W surface exposed to a SF_6 plasma, comparison between vacuum transfer (in situ) and air transfer (ex situ) from the process chamber to the XPS.

to atmospheric exposure. The F 1s distribution shows two contributions: one at 684.7 eV (F–W), results from the fluorination of the W surface, the second at 687.7 eV is very sensitive to atmospheric exposure and has been shown to decrease during the XPS analysis duration [21]: it is assigned to WF_6 molecules trapped on the surface [37]. XPS has been for a long time the only easy-to-use surface analysis method (with Auger spectroscopy). Since 1986, the development of ellipsometry and atomic force microscopy, have brought new surface analysis techniques.

Ellipsometry is probably the only easy-to-use surface analysis method which can be operated in situ and in real time. On the contrary, multiple internal reflection Fourier transform infrared spectroscopy is a very powerful technique [38] but it is rather tricky to implement. Ellipsometry allows real time studies of the surface modification during exposure to the plasma, and after the treatment. Figure 10 shows for example the variation of Ψ and Δ ellipsometry angles upon fluorination of Si in fluorine-based plasmas as a function of pressure and gas mixture [39], thus demonstrating the sensitivity of the technique. Infrared ellipsometry has also been used with success to investigate reaction layer composition and formation on Si in CF_4-based plasmas [40,41], or to monitor patterning [42].

Atomic force microscopy has been up to now only scarcely used by the plasma processing community. Results mainly concern low-resolution measurements, that is modification of the surface roughness induced by the plasma [43,44]. Micro masking effects have been observed when processing Si with a SF_6 plasma beam at low temperature (Fig. 11) and correlated to the multi-layer adsorption of plasma species as observed by XPS [45]. Further development of vacuum techniques should allow high resolution surface probe microscopy measurements on plasma-treated samples, and possibly lead to complementary information on adsorption kinetics, surface density of states.

14.2.4 Fluorine-based plasma chemistry

14.2.4.1 Reactions in the gas phase

Electron impact processes are the main mechanisms for the production of active species.

Ionisation is simple: $CF_4 + e \rightarrow CF_4^+ + 2e$, or dissociative: $CF_4 + e \rightarrow CF_3^+ + F + 2e$ ($E_{th} \sim 15$ eV)

Excitation leads to dissociation: $CF_4 + e \rightarrow (CF_4)^* \rightarrow CF_3 + F + e$ $k_d \sim 10^{-16}$ m^3 s^{-1}, the threshold energy for dissociative electronic excitation being always greater than that for thermal dissociation. In electronegative gases, dissociation is often attaching:

$CF_4 + e \rightarrow (CF_4)^* \rightarrow CF_3 + F + e \rightarrow CF_3 + F^-$

Electronic attachment: $SF_6 + e \rightarrow SF_6^-$ $k_a \sim 6.2\ 10^{-18}$ m^3 s^{-1}, is generally dissociative: $SF_6 + e$ $SF_5^- + F$ $k_a \sim 2.3\ 10^{-16}$ m^3 s^{-1}. Negative ions formed by electron capture on complex molecules have long lifetimes, the lifetime of SF_6^- being estimated as 32 μs [46].

Neutral recombination: $CF_3 + CF_3 \rightarrow C_2F_6$ $k_{nr} \sim 8\ 10^{-18}$ m^3 s^{-1}, produces heavier molecules.

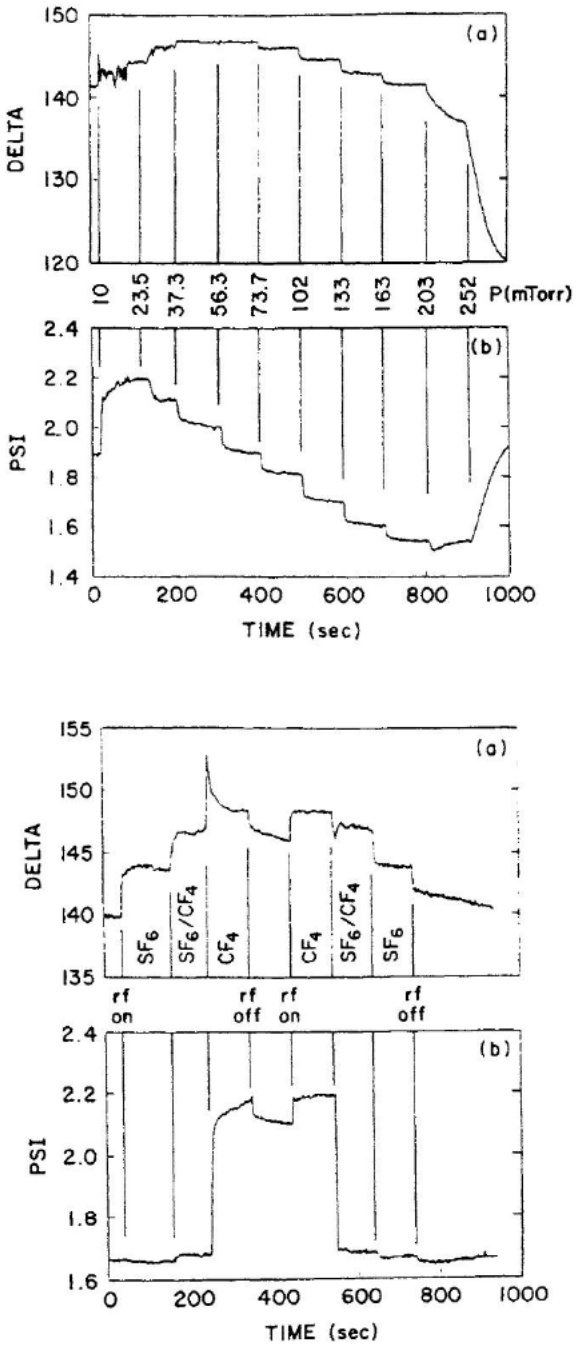

Fig. 10. Ellipsometry analysis in real-time of Si exposed to a CF_4 plasma, Ψ and Δ as a function of pressure or of gas mixture (reprinted with permission from J. Vac. Sci. Technol., A 11 (1993) 34 [39]).

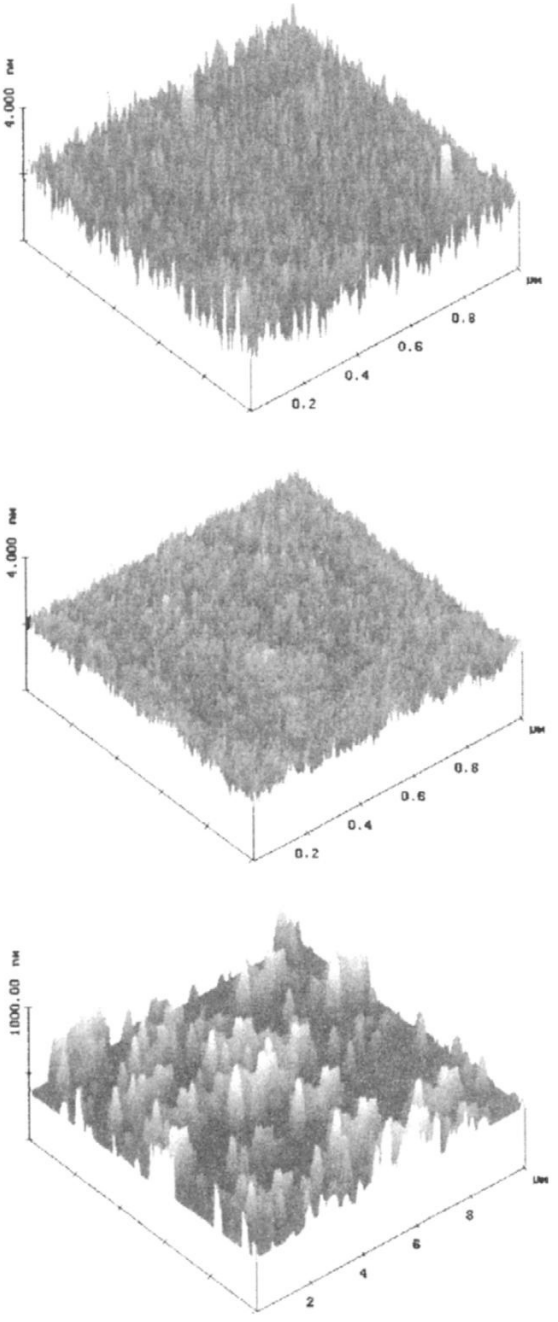

Fig. 11. Si surface aspect after exposure to an SF_6 plasma beam at various substrate temperatures, (top) non-exposed Si; (middle) $T = 230$ K; (bottom) $T = 200$ K. Beam energy is 360 eV, and ion current density 0.65 mA cm^{-2}.

Figure 12 reports electron impact cross sections for CF_4 [47] and SF_6 [48]. In the SF_6 data it should be noticed the very important attachment cross section for the formation of SF_6^- and SF_5^- with low energy electrons [49] which results from the comparable electron affinity of fluorine (3.40 eV) with respect to the dissociation energy of SF_6 (bond strength F—SF_5 = 3.95 eV), whereas the bond strength F—CF_3 is 5.56 eV.

In Table 2 is reported a set of the main reactions predicted to occur in a CF_4 rf plasma [50]. According to the authors, CF_2 radicals could outnumber CF_3 radicals: two fast reactions produce CF_2 from CF_4 (no 2) and CF_3 (no 3) with regard to CF_3 formation (no 1), whereas recombination processes for CF_2 (nos 7 and 8) have a much lower rate than for CF_3 (nos 5 and 6). Experimental results [51] as well as further modelling [52] temper this prediction and give typically a ratio of 1.2 for the relative density of CF_3 with respect to CF_2. On the contrary, absorption spectroscopy analysis [30] is rather in agreement with Fig. 6 and gives a CF_3/CF_2 ratio varying between 5 and 10 with the source power.

14.2.4.2 Effect of additives

The use of gas mixtures enables to vary the composition of the plasma, and often gives more flexibility to optimise the process.

Addition of O_2 to CF_4. Reactions in CF_4—O_2 plasmas have been extensively studied by several authors [53,54]. A well admitted set of reaction is reported in Table 3. Oxygen atoms produced in the discharge react rapidly with the CF_x radicals (reactions nos 21 to 23) by free radical exchange. The products of reaction are relatively stable species (CO, COF or COF_2) and atomic fluorine. This reaction scheme proceeds further (reaction nos 24 and 25) and gives stable molecules (CO_2) and more fluorine, whereas reaction between atomic fluorine and CO or CO_2 have smaller rates (reactions nos 30 and 31). The main effect upon addition of oxygen is thus a strong increase in the concentration of fluorine in the gas phase [55], and a drastic decrease in the CF_x radicals density [56,57] as confirmed by optical diagnostics. The interest for surface fluorination is obvious as it allows to increase the net fluorine flux onto the surface and prevents the formation of fluorocarbon films. A similar increase in the fluorine concentration is observed in the case of SF_6—O_2 mixtures [58].

Addition of H_2 to CF_4. Addition of H_2 to CF_4 leads to the opposite result. The set of reactions given in Table 4 [59] indicates that hydrogen atoms react very rapidly with CF_3 (reaction no 9) and yield stable HF and CF_2. Moreover, fluorine atoms are consumed in reaction nos 20 and 23 with H_2 and H to form HF. The effect of hydrogen addition is thus to decrease the concentration of fluorine (in the plasma jargon people refer to this as the scavenging effect of H_2 in fluorine chemistries) [60], and enhance the density of CF_2 which favours the formation of fluorocarbon films [61]. Many experimental results have confirmed this interpretation [62], examples are given in Figs 13 [63] and 14 [64]. In the particular case of Fig. 13, the authors have observed the F concentration to decrease as the Al electrode is progressively covered with a fluorocarbon layer when increasing the concentration of H_2 in

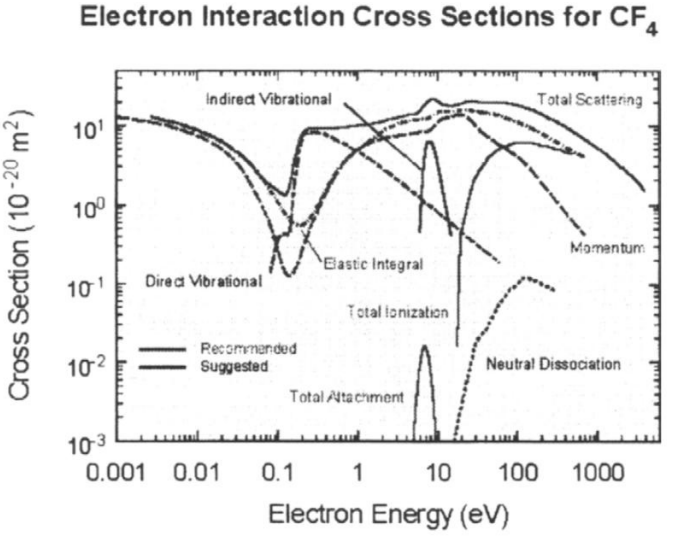

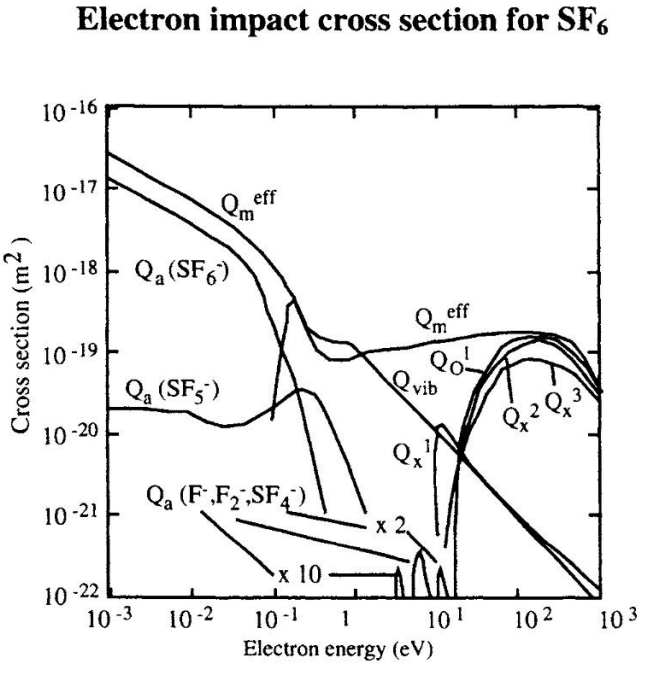

Fig. 12. Experimental cross sections for CF_4 and SF_6 (reprinted with permission from J. Appl. Phys., 64 (1988) 4269 [48] and J. Phys. Chem. Ref. Data, 25 (1996) 1341 [47]).

Table 2

Reaction set in CF_4 plasmas. (Reproduced with permission from Plasma Chem. Plasma Process., 6 (1986) 231 [50]).

Reaction number	Reaction	Rate coefficient at 0.5 Torr
1	$CF_4 \xrightarrow{e} CF_3 + F$	6 s^{-1}
2	$CF_4 \xrightarrow{e} CF_2 + 2\,F$	14 s^{-1}
3	$CF_3 \xrightarrow{e} CF_2 + F$	20 s^{-1}
4	$CF_2 \xrightarrow{e} CF + F$	20 s^{-1}
5	$CF_3 + CF_3 \xrightarrow{M} C_2F_6$	8 10^{-12} cm^3 s^{-1}
6	$CF_3 + F \xrightarrow{M} CF_4$	1.3 10^{-11} cm^3 s^{-1}
7	$CF_2 + CF_2 \xrightarrow{M} C_2F_4$	5 10^{-14} cm^3 s^{-1}
8	$CF_2 + F \xrightarrow{M} CF_3$	4.2 10^{-13} cm^3 s^{-1}
9	$CF + F \xrightarrow{M} CF_2$	5 10^{-15} cm^3 s^{-1}
10	$C_2F_6 \xrightarrow{e} CF_3 + CF_3$	20 s^{-1}
11	$C_2F_4 \xrightarrow{e} CF_2 + CF_2$	20 s^{-1}
12	$F + C_2F_4 \longrightarrow CF_3 + CF_2$	4 10^{-11} cm^3 s^{-1}
13	$CF_2 + CF_3 \xrightarrow{M} C_2F_5$	8.8 10^{-13} cm^3 s^{-1}
14	$C_2F_5 + F \longrightarrow CF_3 + CF_3$	1 10^{-11} cm^3 s^{-1}
15	$CF + CF_2 \longrightarrow C_2F_3$	1 10^{-12} cm^3 s^{-1}
16	$C_2F_3 + F \longrightarrow C_2F_4$	1 10^{-12} cm^3 s^{-1}

Table 3

Additional reaction set in CF_4—O_2 plasmas. (Reproduced with permission from Plasma Chem. Plasma Process., 6 (1986) 205 [53]).

Reaction number	Reaction	Rate coefficient at 0.5 Torr
17	$O_2 \xrightarrow{e} O + O$	6.5 s^{-1}
18	$COF_2 \xrightarrow{e} COF + F$	20 s^{-1}
19	$CO_2 \xrightarrow{e} CO + O$	40 s^{-1}
20	$F_2 \xrightarrow{e} F + F$	20 s^{-1}
21	$CF_3 + O \longrightarrow COF_2 + F$	3.1 10^{-11} cm^3 s^{-1}
22	$CF_2 + O \longrightarrow COF + F$	1.4 10^{-11} cm^3 s^{-1}
23	$CF_2 + O \longrightarrow CO + 2F$	4. 10^{-12} cm^3 s^{-1}
24	$COF + O \longrightarrow CO_2 + F$	9.3 10^{-11} cm^3 s^{-1}
25	$COF_2 + O \longrightarrow CO_2 + F_2$	2.1 10^{-11} cm^3 s^{-1}
26	$F + O_2 \longrightarrow FO_2$	1.8 10^{-16} cm^3 s^{-1}
27	$F + FO_2 \longrightarrow F_2 + O_2$	5.0 10^{-11} cm^3 s^{-1}
28	$O + FO_2 \longrightarrow FO + O_2$	5.0 10^{-11} cm^3 s^{-1}
29	$O + FO \longrightarrow F + O_2$	5.0 10^{-11} cm^3 s^{-1}
30	31	$CO + F \xrightarrow{M} COF$

Table 4

Reaction set in CF_4—H_2 plasmas, at 0.5 Torr (Reproduced with permission from J. Electrochem. Soc., 137 (1990) 2280 [59]).

Reaction number	Reaction	Reaction number	Reaction
1	$CF_4 + e \longrightarrow CF_3 + F + e$	15	$CHF_3 + F \longrightarrow CF_3 + HF$
2	$CF_4 + e \longrightarrow CF_2 + 2\,F + e$	16	$CF_3 + HF \longrightarrow CHF_3 + F$
3	$CF_3 + CF_3 + M \longrightarrow C_2F_6 + M$	17	$CHF_3 + F \longrightarrow CF_4 + H$
4	$CF_3 + F + M \longrightarrow CF_4 + M$	18	$CF_4 + H \longrightarrow CHF_3 + F$
5	$CF_2 + F + M \longrightarrow CF_3 + M$	19	$CF_3 + H + M \longrightarrow CHF_3 + M$
6	$H_2 + e \longrightarrow H + H + e$	20	$F + H_2 \longrightarrow HF + H$
7	$CF_4 + H \longrightarrow CF_3 + HF$	21	$HF + H \longrightarrow F + H_2$
8	$CF_3 + HF \longrightarrow CF_4 + H$	22	$H + H + M \longrightarrow H_2 + M$
9	$CF_3 + H \longrightarrow CF_2 + HF$	23	$H + F + M \longrightarrow HF + M$
10	14	$CF_2 + HF$	$\longrightarrow CHF_3 + H$
11		$\longrightarrow$	$CHF_3 + H \longrightarrow CF_3 + H_2$
12		$CF_3 + H$	$CF_2 + HF + M \longrightarrow CHF_3 + M$
13		$CF_3 + H_2$	$CHF_3 + M \longrightarrow CF_2 + HF + M$

the gas, whereas there is no effect for a PTFE electrode. Moreover, when beginning at 40% H_2 and decreasing the H_2 concentration, the F signal starts at this lower value and stays constant for both materials. This different variation of the relative F concentration, depending on the way the plasma composition is modified reflects the real chemical nature of the electrode surface: Al in the first case, or a stable fluorocarbon layer in the other. This points out the important feedback of wall conditions on the plasma composition which is detailed in the next section.

14.2.4.3 Effect of materials surface

The chemistry of the gas phase is also strongly influenced by the nature of the surfaces (wall or sample) exposed to the plasma. As an example, Table 5 lists the probability of fluorine loss on various materials along different processes [2]. F recombines totally on zinc to form F_2, is chemically inert on alumina, and reacts on Si or BN to form volatile products, thus inducing etching process.

Figure 15 reports experimental results obtained by emission spectroscopy on the relative evolution of the fluorine concentration in CF_4—O_2 and SF_6—O_2 mixtures in a rf diode reactor for various rf electrode materials (Al, Si, Ge) [55,65]. In the case of an electrode material inert with respect to the plasma (Al), addition of O_2 to SF_6 and CF_4 induces, as expected, an increase of the fluorine concentration until the dilution effect lowers the F density. The lower F concentrations observed in the case of Si and Ge electrodes are due to the consumption of fluorine on these surface to form volatile SiF_4 and GeF_4. In the case of Si with SF_6, from 0 to 40% O_2 addition reaction is so fast that it consumes all the additional fluorine produced in the plasma. Above 40% O_2, the F concentration increases gradually to

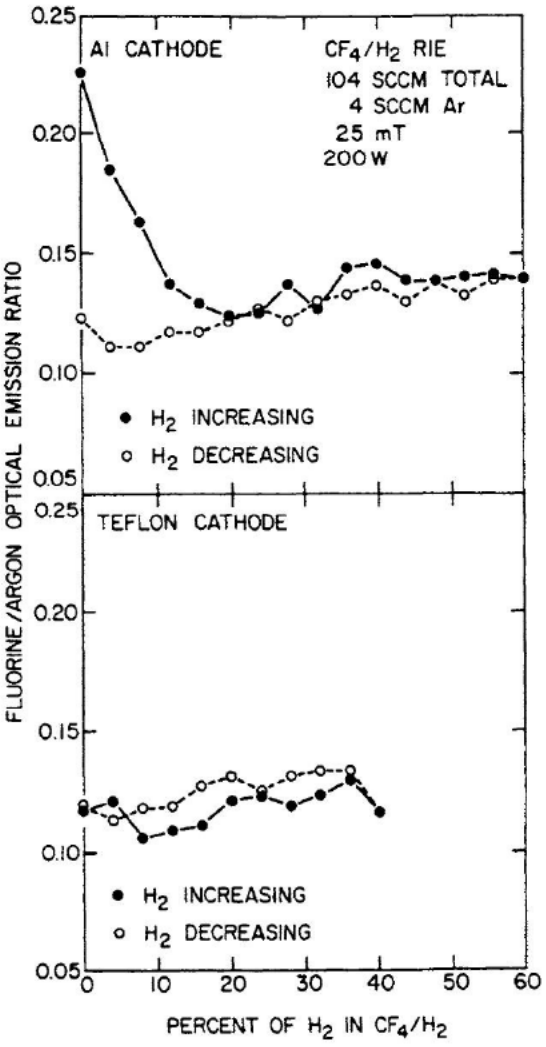

Fig. 13. Effect of fluorocarbon film deposition in CF_4—H_2 mixtures on the F concentration in the gas phase (reprinted with permission from J. Appl. Phys., 62 (1987) 662 [63]).

finally reach that observe for Al: this observation is a strong indication that the Si etching rate has decreased. On the contrary for Ge the evolution of the F density has a bell shape similar to that observed for Al, suggesting that the Ge etching rate remains high even in rich O_2 mixtures.

Gas phase reactions are highly sensitive to surface composition, and therefore processes on chamber material, wall contamination, and history use have an important effect on process chemistry.

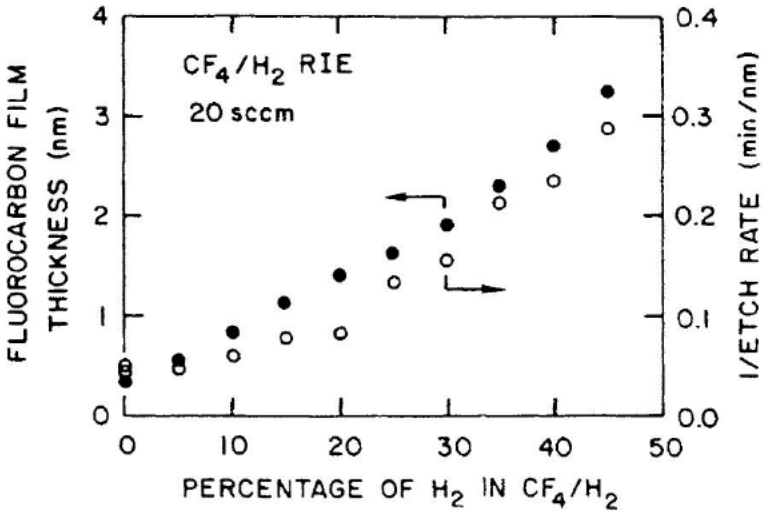

Fig. 14. Fluorocarbon film thickness on Si and Si etching rate as a function of the gas mixture in CF_4—H_2 plasmas (reprinted with permission from Mat. Res. Soc. Symp. Proc., 98 (1987) 229 [64]).

Table 5

Probability for F atom loss on various materials, from [2] p. 115

Material	Temperature, (K)	F atom loss probability	Process	Product
Alumina	300	$6.4\ 10^{-5}$	Recombination	none
Quartz	300	$1.5\ 10^{-4}$	Total loss	SiF_4
Quartz	300	$1.9\ 10^{-5}$	Reaction	SiF_4
Pyrex	300	$1.6\ 10^{-4}$	Recombination	
Steel	300–470	$2.8\ 10^{-4}$	Recombination	
Molybdenum	300	$4.2\ 10^{-4}$	Recombination	
Nickel	300	$7.2\ 10^{-4}$	Recombination	
Aluminum (0.1% Cu)	300–560	$1.8\ 10^{-3}$	Recombination	
Copper	300–570	> 0.011	Recombination	
Brass	300	> 0.05	Recombination	
Zinc	300	> 0.2	Recombination	F_2
Teflon	300	$< 7\ 10^{-5}$	Recombination	
BN	300–500	~ 1	Reaction	BF_3, N_2
Silicon	300	0.0017	Reaction	SiF_4

14.2.5 Surface fluorination mechanisms: concepts and examples

Fluorine-based plasmas are currently employed in microelectronics industry for etching processes of metal (W), semiconductors (Si, Ge), or dielectrics (SiO_2, Si_3N_4). Mechanistic studies have shown that the key parameters of the plasma-surface inter-

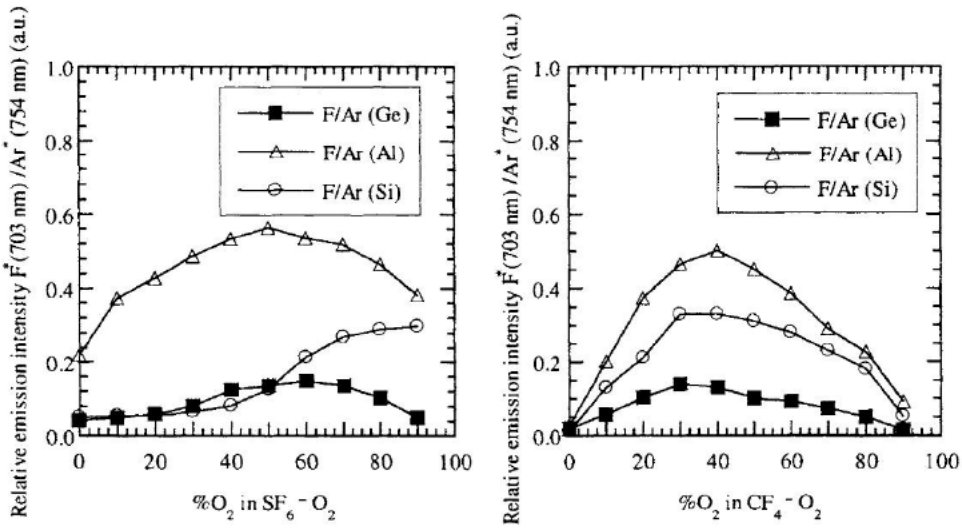

Fig. 15. Fluorine concentration in CF_4—O_2 and SF_6—O_2 mixtures for various electrode materials (reprinted with permission from Plasma Sources Sci. Technol., 4 (1995) 398 [55] and J. Vac. Sci. Technol., B 13 (1995) 235 [65]).

action varies for each material upon the gas mixture and the ion bombardment. Very often the ratio of the neutral flux to ion energy flux is the dominant parameter.

Ion-assisted gas-surface chemistry mechanism is probably the best terminology to describe the plasma processing of a surface. A remarkable illustration of the effect of ion bombardment is reported in Fig. 16 [66]. The reaction rate of XeF_2 with Si increases drastically upon the simultaneous combination of chemical species (XeF_2) and ions (Ar^+) on the surface. Obviously chemical reaction and some sputtering processes are expected to occur and to be responsible of the ablation of the material, but the combined effect of active neutral species and ion bombardment is more efficient than the sum of the individual processes.

14.2.5.1 General concepts of plasma-surface interaction

Spontaneous reactions. In this simple case the reaction rate is expected to be proportional to the flux of active neutral species on the surface. In plasma environment, this mechanisms truly occurs only in post discharge situation when the sample is located downstream with respect to the region where the plasma is created, and suffers no ion bombardment. Studies on the etching of Si and SiO_2 with F_2 plasmas [67] have shown that the reaction rate is proportional to the atomic fluorine density and obeys an Arrhenius law with temperature.

Sputtering. Sputtering is a purely physical process with a yield (atom ion^{-1}) given by the relation: $Y_i A \cdot (\sqrt{E_i} - \sqrt{E_{th}})$ with $E_i > E_{th}$, ~20–50 eV [68] for clean surfaces.

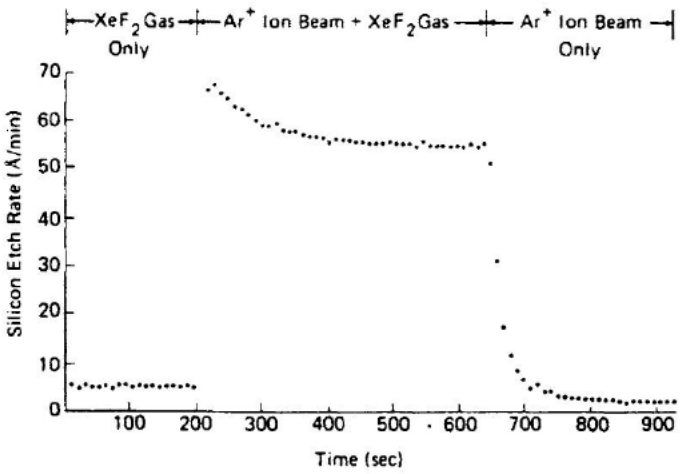

Fig. 16. Si etching rate in ion-assisted gas-surface chemistry mechanisms as compared to pure chemical reaction or ion sputtering (reprinted with permission from J. Appl. Phys., 50 (1979) 3189 [66]).

In plasma environment, the surface chemistry is modified with respect to the initial surface, and the threshold energy and the slope A are found to decrease [69,70]. In this case the terminology "chemical enhanced sputtering" is often used to distinguish this process from the sputtering of a clean surface. Sputtering leads to the ablation of the material, and can concern any surface exposed to the plasma, not only the surface to be processed.

Surface activation. This term covers all processes in which ions essentially bring energy to the surface. This can lead to chemical damage such as broken bonds and create active sites for adsorption of neutral species. Another extremely important process is the activation of adsorbed species, or the activation of surface atoms under the impact of an ion, inducing a chemical reaction. This process is often called "chemical sputtering", but a more correct term seems to be "ion-assisted reaction". It leads to the formation of a weakly bound species which desorbs either spontaneously (spontaneous etching) or under the impact of another ion (chemical enhanced sputtering) [71,72]. It is this process which is responsible for the enhancement of the etching rate reported in the example of Fig. 16.

Damage. Energetic ions can cause damage well below the plasma-sur- face interaction layer. Structural damage concern mostly mono-crystalline materials, the damaged layer can reach 5–9 nm. Light atoms such as hydrogen can diffuse on several hundreds of Å. Materials can undergo strong modification of composition if the resulting product of the interaction is volatile for one element and unvolatile for another. A typical case is that of GaAs which exposed to SF_6 plasmas leads to the formation of volatile arsenic fluoride and leaves a GaF_3-rich layer on the surface [73,74].

14.2.5.2 Elements of surface kinetics

Let us consider the etching of a surface S of material M with F atoms and the volatile product to be MF. With the concepts defined above one can write the following set of reactions.

The first step is the adsorption of fluorine atoms:

- $F(g) + M \rightarrow M : F$, rate : $K_a \cdot (1 - \theta) \cdot n'_F$ adsorption of fluorine atoms,

Adsorption of fluorine on the surface is supposed to obey Langmuir kinetics: θ the fraction of the surface covered with fluorine is smaller than one, with K_a ($m^3\ s^{-1}$) being the adsorption rate constant per fluorine, and η'_F the fluorine concentration in the gas phase near the surface.

The second step is surface reactions:

- $M : F \rightarrow S : MF$ rate : $K_r \cdot \theta$ spontaneous (thermal) reaction to form a product,
- $M : F + ion \rightarrow S : MF$ rate : $K_{iar} \cdot \theta \cdot n'_i \cdot E_i$ ion-assisted reaction to form a product,

with K_{iar} ($m^3\ s^{-1}\ J^{-1}$) the reaction rate constant per ion, and n'_i the ion concentration in the gas phase near the surface. The ion assistance is supposed to combine both ion energy and ion flux as the role of the ion bombardment is to bring energy to the surface.

The third step is product desorption:

- $S : MF \rightarrow S : MF(g)$ rate : $K_d \cdot \theta_1$ spontaneous (thermal) desorpton of a product,
- $S : MF + ion \rightarrow S + MF(g)$ rate : $K_{ces} \cdot Y_{ces} \cdot Y_{ces} \cdot \theta_1 \theta_{ni}$ chemical enhanced sputtering,

with θ_1 the fraction of the surface covered with reaction products and K_{ces} the reaction constant per ion ($m^3\ s^{-1}$).

Direct sputtering can be also considered:

- $M + ion \rightarrow M(g)$ rate : $K_i \cdot Y_i \cdot n'_i \cdot (1 - \theta)$

In a steady state situation, the etching rate is expressed by:

$$ER(\text{atom}\,s^{-1}) = N_M \cdot S \cdot [K_i \cdot Y_i \cdot n'_i \cdot (1 - \theta) + K_d \cdot \theta_1 + K_{ces} \cdot Y_{ces} \cdot \theta_1 \cdot n'_i]$$

or,

$$ER(m\ s^{-1}) = \frac{N_M}{n_M} \cdot [K_i \cdot Y_i \cdot n'_i \cdot (1 - \theta) + K_d \cdot \theta_1 + K_{ces} \cdot Y_{ces} \cdot \theta_1 \cdot n'_i],$$

with n_M the atom density of material M and N_M the atom surface density.

Solving that $(\partial\theta/\partial t) = 0$ and $(\partial\theta_1/\partial t) = 0$ in a stationary regime gives:

$$ER = \frac{N_M}{n_M} \cdot (K_i \cdot Y_i \cdot n_i' + K_a \cdot n_F') \cdot \left[\frac{1}{1 + \frac{K_a \cdot n_F'}{K_r + K_{iar} \cdot n_i' \cdot E_i}} \right].$$

This expression is unusable as it is, but it reduces to some interesting limits for some practical cases. Generally direct sputtering processes are negligible in reactive plasmas with respect to chemical processes, so one can omit the term $K_r \cdot Y_i \cdot n_1'$ and then:

$$ER = \frac{N_M}{n_M} \cdot \left[\frac{1}{\frac{1}{K_a \cdot n_F'} + \frac{1}{K_r + K_{iar} \cdot n_i' \cdot E_i}} \right].$$

This relation shows two interesting limits in the usual situation of plasma processing, that is when the sample is submitted to both ions and neutral species. When $K_a \cdot n_F' \ll K_r + K_{iar} \cdot n_i' \cdot E_i$, the etching is limited by the flux of fluorine atoms on the surface, then $\theta \ll 1$ and

$$ER = \frac{N_M}{n_M} \cdot K_a \cdot n_F'.$$

When $K_a \cdot n_F' \gg K_r + K_{iar} \cdot n_i' \cdot E_i$, the surface is saturated with fluorine, $\theta = 1$ and

$$ER = \frac{N_M}{n_M} \cdot [K_r + K_{iar} \cdot n_i' \cdot E_i].$$

In this latter case the etching rate is thus limited by the ion flux if $K_r \ll K_{iar} \cdot n_i' \cdot E_i$, or by the surface reaction rate in the absence of ion bombardment. Figure 17 shows the evolution of ER and these two limits. In addition, the above relation contains the reason why anisotropic etching (and thus pattern transfer for microelectronics) is achievable in plasma environment. Vertical etching (ER_v) is obtained by biasing the sample such as the ion-assistance prevails on thermal reactions: $K_{iar} \cdot n_i' \cdot E_i \gg K_r$. On another hand, the ion flux on the lateral sidewall of the trench is considered to be zero; this assumption is correct as long as the feature size is smaller than the Debye length so that the sheath edge stays parallel to the macroscopic surface and does not follow the pattern. Then the lateral etching rate (ER_l) corresponds to the case: $K_{iar} \cdot n_i' \cdot E_i \ll K_r$.

This model is quite universal providing that the ion-induced reaction rates prevail on the thermal reaction rates. It has been thoroughly discussed for Si and SiO_2 etching by means of beam experiments [75–77], and has been checked in plasma environment [78]. It is also verified for other systems: Si in Cl_2, [79], SiGe alloys in SF_6 [80], or InP in CH_4—H_2 [81].

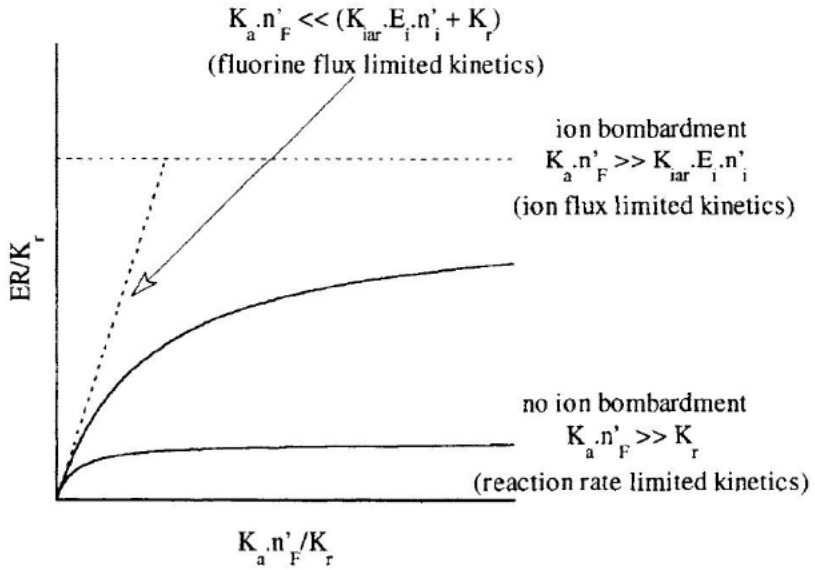

Fig. 17. Predicted evolution of the etching rate as a function of the fluorine density near the surface for a fixed ion energy flux on the surface.

14.2.5.3 Examples of fluorination mechanisms

Diffusion mechanism through a surface layer. A typical example of this situation is that of Si and SiO_2 in fluorocarbon plasmas. In this particular case, a competition exists at the surface between surface fluorination (which further leads to etching) and fluorocarbon film deposition. These systems have been extensively studied in the past years for their capability to give selective etching of SiO_2 over Si. A fluorocarbon film is present at the Si surface, and the reaction rate is inversely proportional to the layer thickness (Fig. 14). This indicates that a diffusion mechanism for the fluorine atoms takes place through this layer in order to account for the reaction with the material surface [64,82]. Moreover, for a given plasma chemistry, the layer thickness and competition is controlled by the ion energy flux on the surface [82,83] as described in Fig. 18. Such a diffusion mechanism is expected to control surface fluorination whenever the plasma phase contains precursors for film deposition. The key parameters which control the equilibrium between fluorination and deposition are two ratios: the F flux-to-CF_x flux ratio, and the ion energy flux-to-CF_x flux ratio. The above set of equation could probably be modified to express this situation with a competitive adsorption mechanism between F and CF_x.

Surface reactivity controlled mechanism. A common example is the fluorination of Si or Ge in SF_6—O_2 or CF_4—O_2 mixtures. As expected from Fig. 15, the reaction rate of Si and Ge increases upon addition of O_2 to SF_6 and CF_4 before decreasing in O_2 rich mixtures. In CF_4—O_2, the reaction mechanism is controlled by the compe-

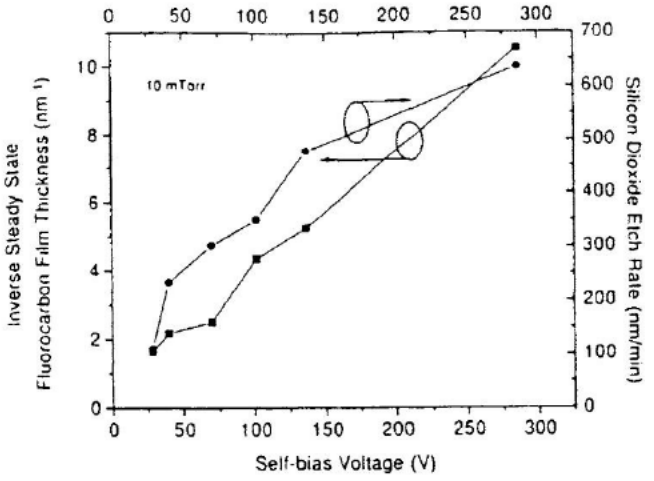

Fig. 18. Dependence of the fluorocarbon thickness on SiO_2 and SiO_2 etch rate with the sample bias voltage (ion energy) (reprinted with permission from J. Vac. Sci. Technol., A 15 (1997) 1881 [82]).

tition between F and O atoms for the occupancy of adsorption sites on the surface [84] with two key parameters: the F/O concentration ratio in the gas phase (n_F/n_O) and the surface reactivity to fluorine atoms. The latter is defined as proportional to the etching rate to fluorine concentration ratio (ER/n_F). Further experiments in SF_6—O_2 and CF_4—O_2, combining optical emission, X-ray photoelectron, and mass spectroscopies, have brought additional information [55,65]. The Si and Ge surface reactivities to fluorine have been determined from both mass spectrometry analysis and etch rates, and surface composition has been evaluated by XPS.

In the case of silicon, the surface reactivity and thus the effective etching rate is directly correlated to the surface chemistry: the formation of an oxyfluoride layer inhibits the reaction. In CF_4—O_2 mixtures, the inverse of the surface reactivity varies linearly with $[n_F/n_O]^{-1}$ as predicted by the model (Fig. 19), the slope being proportional to ratio of the adsorption–desorption rate constant of oxygen on the surface (K_a/K_d). In SF_6—O_2 mixtures a similar situation is observed with two slopes, indicating two regimes. The change of slopes corresponds to the formation of a "thick" oxyfluoride layer (> 10 Å). A further element is the difference in the ion energy flux onto the surface. For the same applied power, the sheath voltage drop on the driven electrode is much smaller (~30–70 V) in SF_6—O_2 mixtures than for CF_4—O_2 (~150–170 V), due to the much higher electron affinity of SF_6-plasma products as compared to CF_4. The following assumption can be proposed: the first slope in the (Si, SF_6) system is weak because fluorine flux is much larger than oxygen flux. The change of slope corresponds to a change of the chemical nature of the surface, adsorption mechanisms then concern an oxyfluoride layer not a clean Si surface. Such a behaviour is not encountered for (Si, CF_4) because

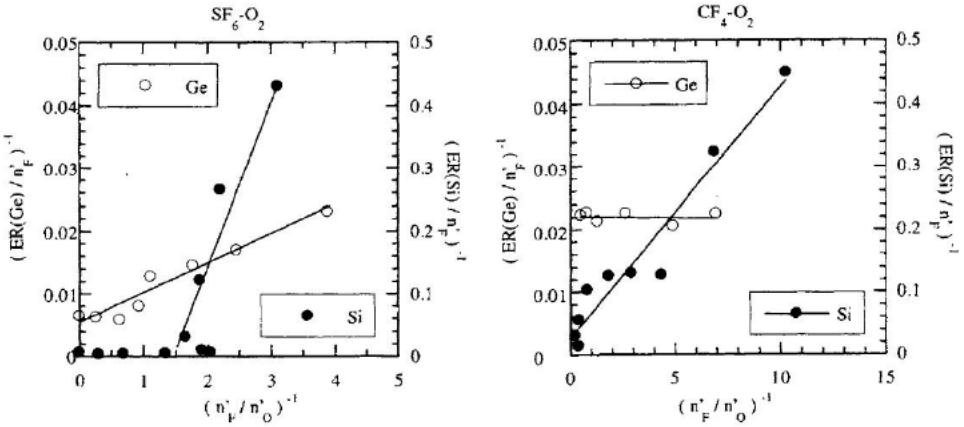

Fig. 19. Inverse of (ER/n_F) as a function of $[n_F/n_O]^{-1}$ for Si and Ge processes in CF_4—O_2 and SF_6—O_2 mixtures.

the ion energy flux is large enough to limit the formation of the oxyfluoride layer and allows surface damage or diffusion of fluorine to the underlying Si surface.

In the case of germanium, the formation of an oxyfluoride layer does not inhibit the etching in SF_6—O_2 mixtures (only one slope), and for CF_4—O_2 there is no dependency of the surface reactivity with the oxygen flux (null slope means $K_d \gg K_a$). Oxygen addition only provokes a modification of the fluorine concentration in the gas phase. Once more the energy brought by the ion bombardment explains these differences.

In conclusion Si etching is essentially controlled by the surface chemistry and diffusion of fluorine through the overlayer, as in the previous example, whereas germanium etching depends mainly on the fluorine flux with a weak effect of the surface chemistry.

Product desorption controlled surface chemistry. Plasma exposure of tungsten in SF_6—O_2 mixtures results in two volatile products WF_6 and WOF_4 [85]. As indicated in Fig. 20 the dominant detected product varies with the nature of the electrode material that is with the atomic fluorine concentration [86] in the gas phase. WF_6 is the detected product in F-rich plasmas and WOF_4 that of F-poor plasmas. XPS analysis on a W plate exposed to SF_6-40% O_2 shows the presence of WOF_4 compounds in addition to O—W, F—W, and SO_xF_y species. Moreover angular XPS analyses indicate that these WOF_4 species are located between the tungsten surface and the oxyfluoride external layer [87]. Reactions between the plasma species (F and O atoms) and the tungsten surface take place at the W-overlayer interface, after diffusion of these species through the overlayer.

Interpretation is that WOF_4 is probably the dominant product formed at the tungsten surface in SF_6—O_2. The nature of the final product desorbed in the gas phase depends on the fluorine and oxygen concentration in the gas phase. If these fluxes are high (as in the case of a plasma-insensitive electrode material, such as

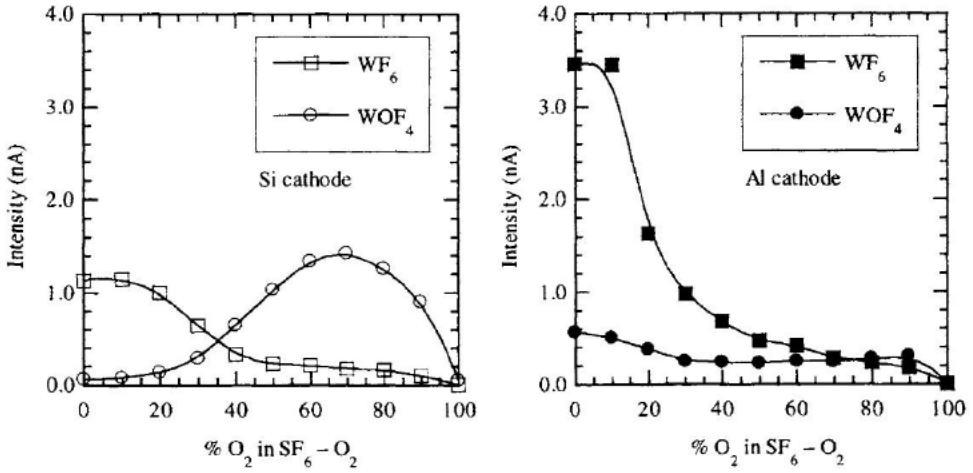

Fig. 20. Intensities of WF_5^+ (WF_6) and WOF_3^+ (WOF_4) signals detected in SF_6—O_2 plasmas.

Al), the slow desorbing WOF_4 species react with the incoming plasma species and the final product is dominantly WF_6 even though there is oxygen in the gas phase. This mechanism is accompanied by the formation of WO_xF_y species which maintains the overlayer. This explains the slow elimination of the oxide and the high fluorine concentration reported in Fig. 7 during oxide elimination. If these fluxes are low (as in the case of a plasma-reactive electrode material, such as Si or W), few reactions occur during the diffusion of WOF_4 in the overlayer, resulting in desorption of this product in the gas phase, and the overlayer is reduced to a minimum.

14.3 Part II: Examples of surface modification of inorganic materials

14.3.1 Surface modification in plasma-enhanced fluorination (PEF) conditions

14.3.1.1 Modification of surface properties of graphite

Graphite-based materials are nowadays involved in a very wide range of systems. They are used as bulk products or are combined with other components to form composite materials. The improvement of the properties of these systems mostly depends on the modifications that occur at the surface: for example, the mechanical behavior is dependent on the quality of the fiber/matrix interface and the water repellency is improved when the surface free-energy is reduced.

Graphite fluorides are solids of low surface energy and good thermal stability. They have been used as moisture resistant lubricants, water repellents and lithium battery cathodes [89]. Since many of the uses of graphite fluorides thus depend on their surface properties, surface fluorination of graphite materials has been expected to give rise to similar behavior. The methods that had been used in the past for implanting F-containing groups onto polymers through fluorinated

plasmas, have been therefore adapted to various type of graphite materials: bulk, flakes, fibers, powders. rf plasmas at 13.56 MHz and electron cyclotron resonance plasmas with rf-induced negative self-bias voltage have been mostly used with various fluorinated gases such as F_2, NF_3, CF_4, SF_6. It can be noted that depending on the experimental conditions, the fluorination could go to completion and bulk graphite fluoride could be obtained from graphite flakes treated in F_2 plasma at 20 MHz [90].

The hydrophobic nature of F-treated graphite can be evaluated from contact-angles of liquid droplets. The surface free-energy can be reduced from 50 mJ m^{-2} to as low as 7 mJ m^{-2} after exposure to NF_3 or SF_6 rf plasmas. A significant coverage of surface fluorination is achieved for exposure times of 10–15 min under an NF_3 plasma, yielding water contact angle of 115° [91]. In some case this value has been found to exceed that of PTFE [92].

In DC discharge plasmas, the sudden decrease of contact angle after 15 min treatment has been assigned by S. Okasaki et al. to a structural change of the material surface from crystallised graphite to an amorphous state [93]. It has been shown that the fluorination of PAN-based carbon fibers is more effective in the case of CF_4-He plasmas than in 5% F_2—He plasmas [94]. The study of the thermal stability of these F-treated fibers has shown however that a 70% loss of fluorine occurred when the samples were heated at 293°C for 10 min.

14.3.1.2 Influence of the morphology of carbon materials on the nature of C—F bonds

The nature of C—F bonds that are formed during the reaction between F species and C materials depends on two main factors: (i) the experimental conditions of fluorination (low-pressure plasmas, F_2-gas, fluorinated media); and (ii) the physicochemical characteristics of the pristine materials (graphitisation level, morphology).

The influence of the experimental conditions has been extensively studied for the bulk fluorination of graphite by F_2-gas in particular by N. Watanabe, T. Nakajima and H. Touhara [89,95]. When the thermal energy brought to the system is large enough ($T_{F_2} > 350$°C), the fluorination gives rise to the formation of covalent C—F bonds with sp^3C, as for instance in the case of the graphite fluoride $(CF)_n$. On the other hand, when the fluorination is carried out at low-temperature ($T_{F_2} < 100$°C), in the presence of additive or catalytic species, intercalation of F between the graphitic layers occurs, without modification of the sp^2 configuration of C [96]. In the corresponding graphite intercalation compounds (GICs) of C_xF formulation, the C—F bonds have been called "semi-ionic" after N. Bartlett et al. [97]: in the XPS spectra, these latter contributions take place at BE lower than those of covalent C—F bonds [98] Fluorination of the internal surface of nanotubes has been recently achieved, the C atoms at the external surface retaining the sp^2 hybridization [132]. The influence of the physicochemical characteristics of the starting material on the surface modification will be illustrated below by two different types of carbon compounds: a highly graphitised material, i.e. exfoliated graphite, and a furnace carbon black (Corax N 115), in which the coherence length

of the ordered domains is limited to a few nm. Usual PEF conditions have been defined by F. Moguet [99]: inlet CF_4 flow $= 8 \leq Q\ (cm^3\ min^{-1}) \leq 16$; total pressure $= 25 \leq p\ (mTorr) \leq 200$; rf power $= 40 \leq P\ (W) \leq 110$; reaction duration $= 10 \leq t$ (min) ≤ 300. It can be noted that in these treatments O_2 was not added to CF_4, because in several cases it might lead to an important etching of the materials.

PEF treatment of exfoliated graphite. The dependence of C_{1s} and F_{1s} XPS spectra of exfoliated graphite with the duration of plasma treatment is shown in Fig. 21 [99]. In the C1s envelope of the XPS spectrum, the component that corresponds to the graphitic contribution (component 1) remains unchanged after plasma treatment. It is the majoritary component of the spectrum. Due to an asymmetry towards higher BE, this band can be fitted into two peaks at ca 284 and 285 eV [this asymmetry, which is common in metallic sampler, is due to the interactions between the created positive core holes and the conduction electrons]. The second peak could also correspond to surface defect, C—H, and C—O groups. The components appearing for $285 < E_b\ (eV) < 287$ can be assigned to the inductive effect of C—F bonds. They correspond to C atoms that are not directly bound to F atoms, but that are first neighbors of C—F_n groups. In the case of graphite, this contribution is weak because the number of reactive sites (i.e. surface defects and borders of graphitic domains) is limited. We will see that the results are totally different for carbon black samples.

The component at ca 287 eV (component 3) can be assigned to "semi-ionic" C—F bond of intercalated F species, and those at $E_b > 288$ eV to C atoms covalently bound to F atoms. The component at ca 289 eV (component 4) has been correlated to the fluorination of defects present at the surface or in the subsuperficial zone of the graphitic domains. In this case, the sp^2 configuration of C is maintained. The contribution at higher BE (component 5) may arise from different sources: fluorinated domains in which the graphene layers are buckled as in the covalent graphite fluoride $(CF)_n$, or perfluoro groups CF_n with $n = 2$ or 3 present at the peripheral border of graphitic domains.

The evolution of XPS spectra, given in Fig. 21 shows that the contribution of pristine non-functionalised C atoms remains majoritary, whatever the duration of the plasma treatment. The most noticeable change is the increase of the component (4) corresponding to covalent C—F bonds which are formed by the interaction of $F^\bullet$ radicals with the reactive sites of the material, i.e. surface defects, hydrogenated/oxygenated C atom, borders of the graphitic domains. When all these surface sites are fluorinated, the surface is saturated, what is accounted for by the value of C/F ratio of 3.2 obtained for $t \geq 120$ min [99].

The differences between surface fluorination, as obtained by PEF, and bulk fluorination, as obtained by F_2-gas [experimental conditions: 10 bar $F_2 + 0.2$ bar HF; reaction temperature 25°C; reaction duration: up to 3 d] are clearly evidenced in Fig. 22 and in Table 6. The latter route gives rise to a bulk stage-1 GIC of $C_{3.5}F$ formulation and a repeat distance $I_C \sim 0.55$ nm [100]. In both cases, the surface C-to-F ratio is more or less similar: 3.1 and 2.8 respectively. However, in the case of surface fluorination, F-intercalated contribution is almost absent, whereas it

is the main C—F contribution in the case of the GIC $C_{3-5}F$. The information deduced from $F1_s$ spectra is also in good agreement with this result. The envelopes are formed in both cases of two contributions (Fig. 21): the ones at 685.6 eV correspond to F atoms intercalated between the graphene layers (GIC) and the ones

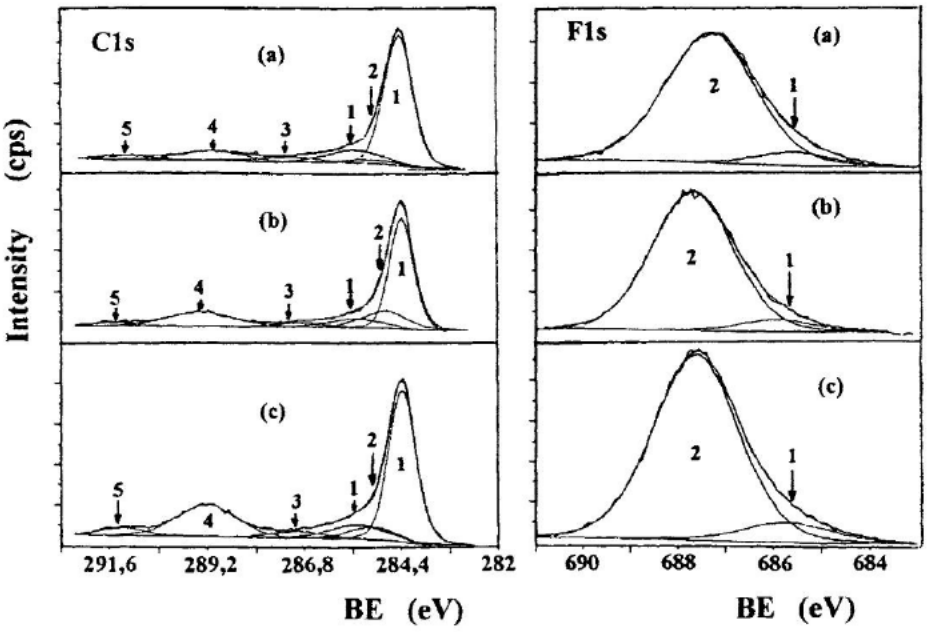

Fig. 21. C1s and F1s XPS spectra of CF_4-plasma treated exfoliated graphite (Experimental conditions: 8 cm^3 min, 200 mTorr, 80 W, 15 min (a), 60 min (b), 120 min (c)).

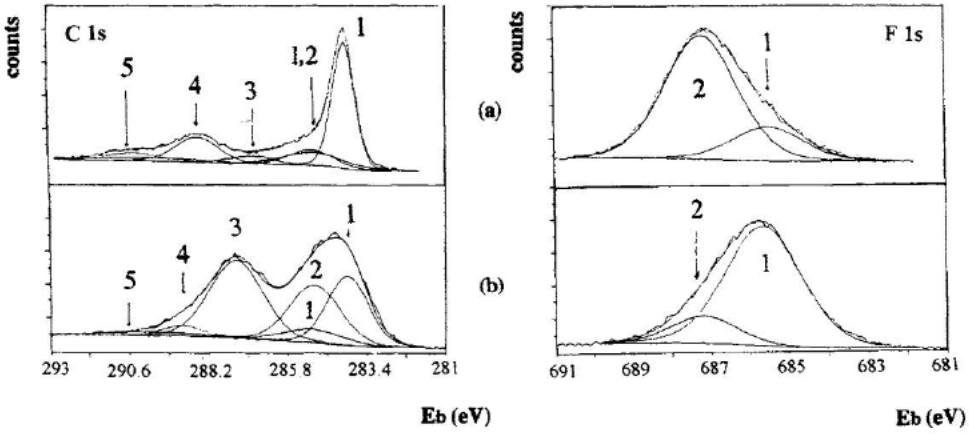

Fig. 22. Comparison of C1s and F1s XPS spectra of fluorinated exfoliated graphite: (a) surface-treated under PEF conditions; (b) GIC ($C_{3.5}F$) obtained under F_2-gas conditions.

Table 6

C1s and F1s binding energies and relative amounts* of carbon and fluorine in fluorinated exfoliated graphite (1.7% O is also found at the surface)

Exp. Conditions	C1s binding energies (eV)	F1s binding energies (eV)	Assignment of the components
CF_4 in rf plasma conditions	284.2 (42%)		Graphitic C
	285.2 (7%)		Asymmetric component
	287.0 (4%)	685.6 (6%)	"Semi-ionic" C—F bond
	288.7 (11%)		Covalent C—F bond (surface defects)
	290.6 (4%)	687.3 (24%)	Covalent C—F bond (similar to graphite fluorides)
F_2-gas under 10 bar pressure (+0.2 bar HF)	284.1 (25%)		Graphitic C
	285.1 (18%)		Asymmetric component + inductive effect of C—F bonds
	287.4 (26%)	685.7 (22%)	"Semi-ionic" C—F bond
	289.1 (3%)	687.3 (4%)	Covalent C—F bond

*The percentages are only indicative because of the uncertainty in the theoretical curve intensities due to the non-equivocal curve fitting.

at 687.3 eV to covalent F—C bonds. The PEF treatment concerns only a very thin layer of the surface of the sample, as shown by a rapid decrease of the F contribution after Ar sputtering. The type of bonds that are formed between C and F atoms is essentially covalent, and only a small amount of fluorine is intercalated. Compared to F_2-gas bulk fluorination, this method allows the formation of a covalent and insulating layer at the outermost surface only, which may act as an efficient protective coating.

PEF treatment of carbon blacks. Due to their important specific surface areas, that range from a few m^2/g to several thousands m^2/g, carbon blacks react thoroughly in PEF conditions. The reactivity of various types of carbon blacks with F_2-gas and other fluorinated reagents has been recently investigated by G. Nansé et al. [101–103].

We have chosen to present below the results obtained on furnace carbon black N115, because of its intermediate surface area of 145 $m^2\ g^{-1}$. The fitted high resolution XPS spectra of C1s and F1s components are given in Fig. 23. Due to the complexity of the morphology of carbon blacks, ten components were required, in order to take into account the envelope of the C1s spectra. Details of the fitting procedure can be found in [101]. The different assignments for C and F atoms involved in each component are shown in Table 7. For C1s envelope, there are two major peaks. The peak at lower BE, located at 284.3eV, can be assigned to the component C1s (1) which corresponds to non-functionalised sp^2 and sp^3 C atoms that are not affected by fluorination. The area of component (1), which is noted

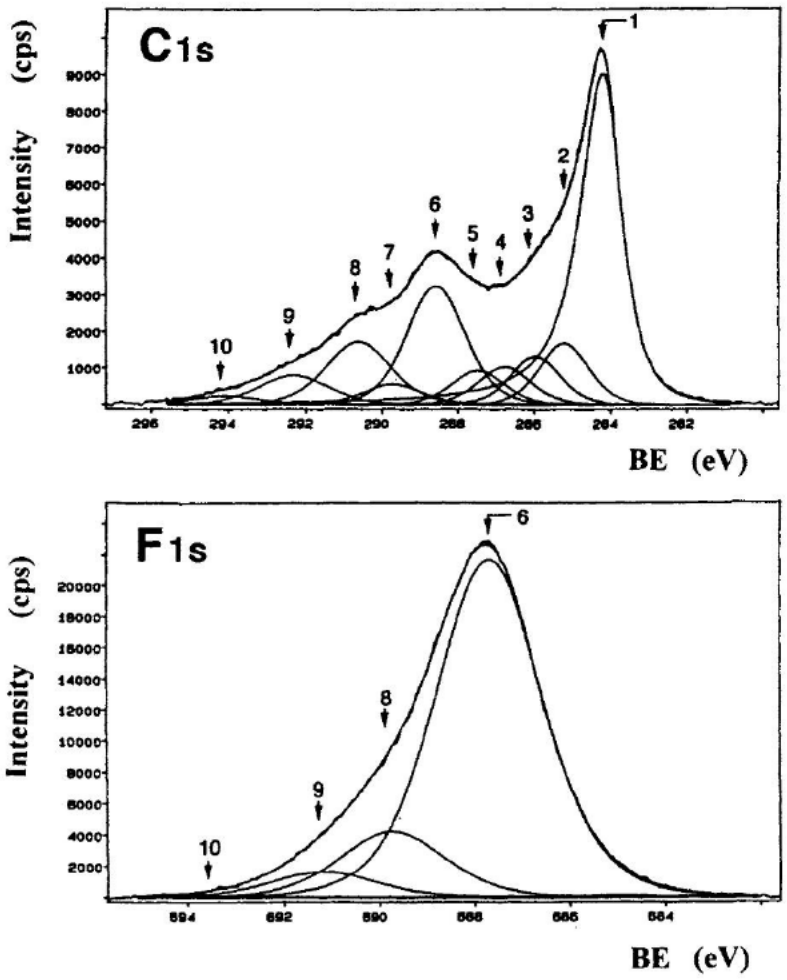

Fig. 23. Fitted high resolution C_{1s} and F_{1s} XPS spectra of plasma-fluorinated furnace carbon black (N115).

AC 1s (1), represents 42% of the total area of the C 1s envelope. This peak has been taken as an internal reference to define the energy separation with the other (i) components: $\Delta C_i C_1$. Areas of the different components and energy separation are collected in Table 8. The peak at higher BE, $C1_s$ (6), which is located at 288.6eV and which is the most important component of C—F bonds, has been assigned to carbon atoms that *are covalently linked to a fluorine atom at the surface and border of the graphitic domains of carbon blacks without any change in the sp^2 conformation of carbon in the bulk* (*Type I structure*). Consequently, the C—C bond length does not differ significantly from that of the initial carbon. Between components (1) and (6) the envelope can be fitted into 4 components corresponding to C atoms that

are not directly bound to F atoms. The shift induced by the presence of F atoms in β position of a given C atoms, i.e. bound to its first neighbors, has been evaluated to about 0.6 ± 0.2eV [102] and is roughly additive. The assignment of these components are given in Table 7.

Table 7

Energy shifts and assignments of the different components of C1s and F1s XPS spectra of PEF-treated N115 carbon black

Component	ΔC_iC_1 (eV)	Assignment
C_1	–	Non-functionalised sp^2 and sp^3 C atoms, not affected by fluorination
C_2	1.0	Aliphatic non-functionalised sp^3 C in a non-fluorinated environment (areas modified by "plasma effect") Non-functionalised sp^2 C in β position to one F atom
C_3	1.8	Non-functionalised sp^2 C or sp^3 C in β position to one or two F atom(s), respectively sp^2 C bound to an oxygen atom (phenol, phenyl ether)
C_4	2.6	Non-functionalised sp^2 C or sp^3 C in β position to two or three F atoms, respectively Oxygenated sp^3 C in a non-functionalised environment (CH_x—OH, or C—O—C)
C_5	3.3 ± 0.1	Oxygenated sp^3 C in β position to a F atom Non-functionalised sp^3 C in β position to at least three F atoms sp^2 C "semi-ionic", bound to intercalated F atom (very week contribution)
C_6	4.2 ± 0.2	sp^2 C covalently linked to an F atom in Type I structure
C_7	5.4 ± 0.3	CF groups of Type I structure in β position of CF_2 groups
C_8	6.3 ± 0.4	CF_2 groups of Type I structure CF groups of Type II structure
C_9	7.9 ± 0.4	CF_3 groups of Type I structure CF_2 groups of Type II structure
C_{10}	9.6 ± 0.4	CF_3 groups of Type II structure Plasmon

Component	ΔF_iF_1 (eV)	Assignment
F_6	–	F atoms in Type I structure
F_8	2.0 ± 0.1	F atoms in Type II structure
F_9	3.5 ± 0.1	F atoms in Type II structure with charge effect
F_{10}	5.9 ± 0.1	F atoms in Type II structure with higher charge effect

Table 8

BE shifts of the different components of C1s and F1s XPS spectra of PEF-treated N115 carbon black

Component	ΔC_iC_1 (eV)	AC 1s (i) (%)
C_1	–	43
C_2	1.0	7
C_3	1.8	6
C_4	2.6	5
C_5	3.3	4
C_6	4.4	17
C_7	5.5	2
C_8	6.4	10
C_9	8.1	5
C_{10}	9.9	1

Component	ΔF_iF_6 (eV)	AF1s (i) (%)
F_6	–	79
F_8	2.1	15
F_9	3.5	5
F_{10}	5.9	1

The components C1s (i), with $i \geq 6$, are attributed to carbon atoms that are covalently bound to F. The amount of such C in the layer explored by XPS can be evaluated from the ratio $\Sigma\, AC1_s(i)\ (6 \leq i \leq 10)/\Sigma\, AC1_s$ (total). This ratio is equal to 36%. In order to identify the components shifted by the charge effect and to differentiate the various forms of fluorinated C that constitute the C_{1s} (i) ($i \geq 6$) components, the $F1_s$ peak was taken as a reference. As a matter of fact, the chemical shift of $F1_s$ core level is less dependent on the x value of CF_x groups than the C core level. In Type I fluorinated structure [i.e. where F atoms are covalently bound to the C atoms of the surface or subsuperficial zones of particles which keep their graphitic character] F atoms belonging to either CF, CF_2 or CF_3 groups contribute to the same component of the spectrum. This component, F1s (6), is located at 687.6eV, and the difference in BE between corresponding components (6) of the F1s and C1s spectra is: $\Delta F_6C_6 = 399.1$ eV. F atoms of CF, CF_2 and CF_3 groups belonging to polyalicyclic perfluorinated structures of Type II (see below) contribute to the same component, $F1_s$ (8). This component is shifted by 2.0 eV relative to F1s (6) in the direction of increasing BE. The corresponding fluorinated entities are those with the highest BE. Consequently, the components with even higher BE, i.e. with $i > 8$, can be attributed to fluorinated domains in which the charge effect is particularly important.

Covalent bonding which is formed between C and F atoms modifies locally the electrical conductivity of the sample. In other words, the key-point will be the extension of the thickness of the fluorinated islands. When the dimensions of these domain increase, the positive space charges that appear in these areas during the photoemission process can be only partially neutralised by photoelectrons and secondary electrons emitted from neighboring or underlying non-functionalised areas. The value of the BE separation between component (1) and high-energy components of C1s spectrum, i.e. $\Delta C_i C_1$, with $i \geq 6$, will thus depend on the degree of fluorination of the sample. The component C1s (7) at 289.8 eV corresponds mostly to CF groups of Type I with CF_2 groups as nearest neighbors. F atoms of these groups are assigned to component (6) of the F1s spectrum. The peak whose fitted component is located at 290.7 eV, C1s (8), can be attributed to CF_2 groups of fluorinated structure of Type I, whose F atoms contribute to F1s (6), and also to CF groups of polyalicyclic perfluorinated structures of *Type II, in which* sp^3 *C skeleton forms puckered layers similar to those of covalent graphite fluorides* $(CF)_n$. F atoms of this second type contribute to the component (8) of $F1_s$ envelope. Shoulder peak (9) and (10) correspond mostly to CF_n groups of Type II and are associated with components (9) and (10) of F1s [see Table 7]. The corresponding zones are strongly affected by charge effect. From the analysis of the XPS spectra of fluorinated, N115 carbon black samples we conclude that all fluorine atoms, fixed at the surface and in the subsuperficial zone of the carbon black particles, are covalently linked to carbon atoms. The majority of the structures of the fluorinated islands present at the surface is of Type I, a structure in which the planar conformation of the graphene layers is preserved. However fluorinated islands of Type II structure also exist at the surface and some of them show a significant charge effect.

As a concluding remark, it is possible to modify the nature of the fluorinated film which is formed on the surface of the carbon black by acting either on the nature of the host material or on the characteristics of the plasma. Concerning the physical properties, it can be expected that the formation of a fluorinated insulating layer on the surface of the carbon blacks increases the repulsion effect between the particles. The electrical contacts between the aggregates become therefore limited and the electrical permittivity, which primarily depends on the number of particles, should be increased.

14.3.1.3 Modification of surface properties of high T_C cuprate superconductors

In 1986, the discovery of high-temperature superconducting cuprates (HTSC) has let to unprecedented activities in numerous scientific fields, mainly because of the possible use of these materials for important technological achievements. Unfortunately the use of bulk HTSC was limited by their relatively low capacity for carrying high densities of electrical current, which is due to several serious material problems such as weak links that are generally present at grain boundaries. It has been shown that a fluorination treatment by F_2-gas contributes to remove impurities from grain boundaries [104], and to protect the material against moist air [105]; in addition the critical current density J_C could be increased. Unfortunately this process affords little indus-

trial adaptability due to drastic safety precautions. In addition, due to the extreme reactivity of F_2, the treatment may easily proceed to a complete fluorination of the materials to insulating fluorides. In order to obtain a surface modification of these ceramics, rf-PEF has been proposed as an alternative processing [107].

Experimental procedures and XPS analysis. Pelletised samples of $YBa_2Cu_3O_{7-\delta}$ containing few residual carbonated species were heated at 920°C under an oxygen flow and slowly cooled under oxygen in order to achieve the optimum oxidation and to limit the cracks formation. The ceramics consisted of homogeneous grains of around 3 μm diameter with an interconnected porosity of about 0.88. Even under these conditions, an amorphous layer was observed by TEM at the gas/solid interface that could be attributed to the presence of surface carbonate [106]. The superconducting properties of these materials have been shown to be improved by PEF treatments involving mixtures of CF_4 and O_2 gases [107,108]. Both values of the resistivity in the normal state (ρ) and of the superconducting transition width (ΔT_C) are reduced and the critical transition temperature (T_C) is increased of about 1 K. The investigation of the various experimental parameters of the process has shown that the improvement of the critical current density (J_C) mainly depends on the inlet precursor composition $CF_4 + x\%\ O_2$, on the total pressure, and on the reaction time. The experimental conditions have been optimised as follows: inlet precursor composition: $CF_4 + 25\%\ O_2$; CF_4-gas flow: 60 $cm^3\ min^{-1}$; total pressure: 225 mTorr; rf power 50–100 W; reaction duration: 30 min. The improvement of the superconducting properties (Fig. 24(a)) is also supported by the decrease of the electrical resistivity in the high temperature domain (Fig. 24(b)).

Mechanisms of interaction between the reactive species of the plasma and $YBa_2Cu_3O_{7-\delta}$ ceramics have been proposed through detailed X-ray photoelectron spectroscopic analyses. Two different types of informations could be obtained from these experiments. The first one concerns the interaction of the reactive species (F_2 or $F^\bullet$) with the grains at the external surface of the pellets. The second one deals

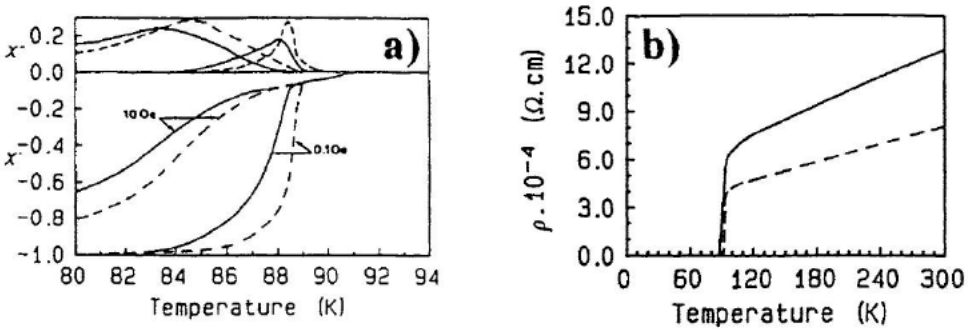

Fig. 24. Improvement of the superconducting properties of $YBa_2Cu_3O_{7-\delta}$ ceramics by PEF processing: (a) a.c. susceptibility curves before (——) and after (- - -) treatment; (b) temperature dependence of the resistivity before (——) and after (- - -) treatment.

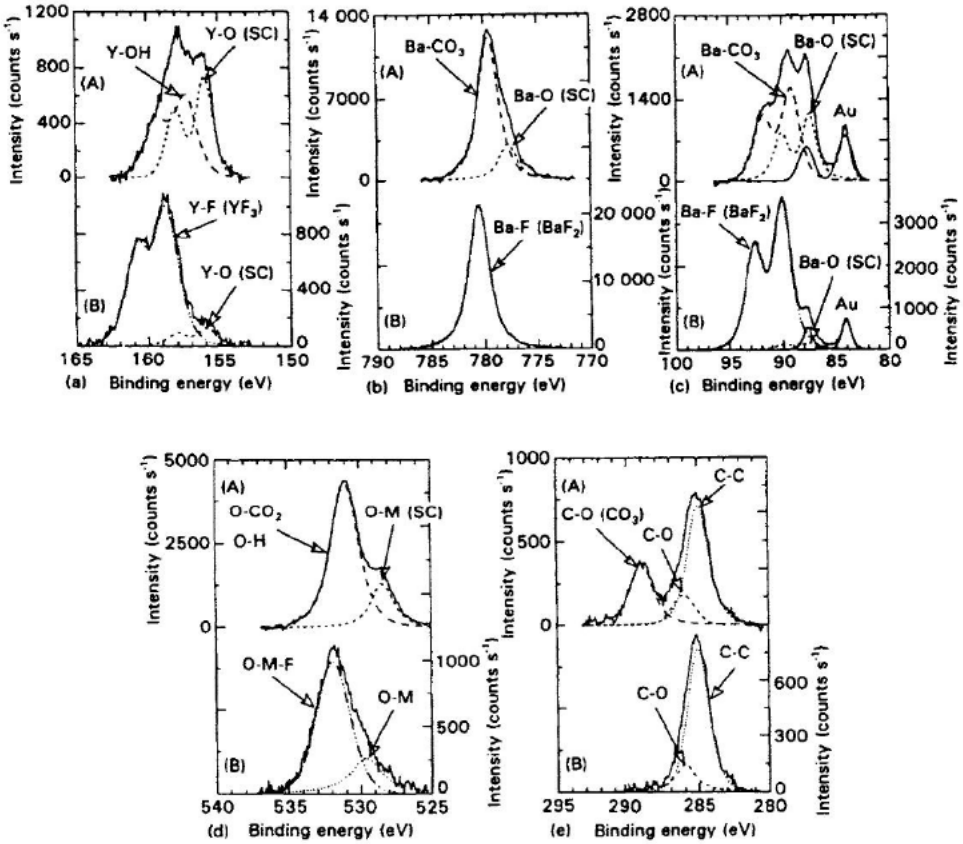

Fig. 25. Y 3d, Ba $3d_{5/2}$, Ba 4d, O1s and $C1_s$ XPS spectra obtained at the surface of the outer grains of the $YBa_2Cu_3O_{7-\delta}$ ceramics before (A) and after (B) the $CF_4 + 25\%$ O_2 plasma treatment (the peaks of the superconducting phase are noted S.C.) (reproduced with permission from J. Mat. Sci., 29 (1994) 4260 [108]).

with the interaction between these species and the surface of the inner grains of the ceramics through the study of polished fractures. During the XPS measurement Cu is partly reduced to monovalent species, as already observed in other Cu-based superconductors [109]. Therefore the XPS study concerns only Y 3d, Ba $3d_{5/2}$, Ba 4d, O 1s and F 1s levels.

Interaction of the reactive fluorinated species with the surface of outer grains of the $YBa_2Cu_3O_{7-\delta}$ ceramics. As shown in Fig. 25(a) before fluorination, Y and Ba XPS spectra of $YBa_2Cu_3O_{7-\delta}$ ceramics are currently characterised by two types of contributions. The binding energies of the so-called "superconducting peaks" are strongly shifted towards lower Eb values. They are attributed to metal–oxygen bonds corresponding to the $YBa_2Cu_3O_{7-\delta}$ lattice [110]. The second type of contribution corresponds to the degradation layer (Y—OH and Ba—CO_3) [111].

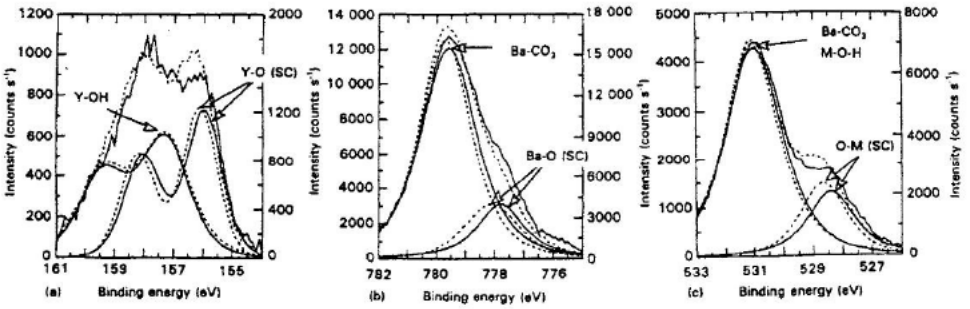

Fig. 26. Y 3d (a), $Ba3d_{5/2}$ (b) and O 1s (c) emission spectra obtained at the surface of the inner grains of the $YBa_2Cu_3O_{7-\delta}$ before (——) and after (- - - -) the $CF_4 + 25\%$ O_2 plasma treatment (reproduced with permission from J. Mat. Sci., 29 (1994) 4260 {108]).

After plasma treatment both peaks of Y and Ba elements corresponding the superconducting phase and to the degradation layer have disappeared from the surface of the outer grains of the ceramics (Fig. 25). New peaks are observed at 158.9 eV (Y 3d), 780.2 eV (Ba $3d_{5/2}$) and 90.0 eV (Ba 4d). They can be unambiguously ascribed to metal–fluorine bonds (as already observed in the case of the F_2-gas treatment [112]). These observations are supported by the presence of an unique F1s peak at 684.7 eV corresponding to fluorine–metal bonds. Contrary to the F_2-gas treatment, the PEF process removes the $(OH)^-$ and $(CO_3)^{2-}$ species without getting $(CF)_n$ and HF_2^- species. The following assumption can be proposed: the interaction of $F^\bullet$ species with the carbonate degradation layer would lead to the formation of volatile compounds like COF or COF_2.

Interaction of reactive fluorinated species with the surface of inner grains of $YBa_2Cu_3O_{7-\delta}$ ceramics. After the PEF treatment, the peaks corresponding in the Y 3d and Ba $3d_{5/2}$ spectra to the superconducting component and to the degradation layer do not change in intensity, and no new peak appears in the high BE domain, as shown in Fig. 26. These observations suggest that the PEF treatment does not decompose the surface of the inner grains, as observed for F_2-gas fluorination. Unfortunately the fluorine content that is distributed homogeneously in the sample has been previously determined by EPMA to be around 0.5 atm%, i.e. too small to be detected by XPS. However it can be pointed out that the peaks corresponding to the components of the superconducting phase are slightly shifted towards higher binding energy (+ 0,2 eV). These displacements cannot be attributed to a charge effect since the BE of the peaks corresponding to the degradation layer remains unchanged. The following assumption has been proposed to explain this behavior: metal–fluorine bonds would be present inside the superconducting phase and the slight shift observed ($\approx$0.2 eV) towards higher BE for the superconducting components of the peaks Y 3d, Ba $3d_{5/2}$ and Ba 4d, would be assigned to an increase of ionicity of the corresponding bonds. The effect of PEF would thus correspond to an increase of the anion rate up to 6.83, which is the content required for optimised

superconducting properties (T_C and J_C) [107]. The treatment removes from the surface of outer grains the $(OH)^-$ and $(CO_3)^{2-}$ species located on the degradation layer of the materials and gives rise to the formation of an homogeneously fluorinated layer, about 7 nm. On the other hand, the PEF treatment does not seem to produce a fluorine rich layer at the surface of inner grains of the materials, but rather leads to the formation of metal-fluorine bonds inside the superconducting phase due to an oxidation process by F species. This effect results in an improvement of weak link behavior of the grain boundaries within the ceramics.

14.3.2 Surface modification in various fluorinating conditions

14.3.2.1 Passivation of metallic surfaces

In order to increase the protection and hydrophobicity of aluminum surfaces, a fluoride film having a high contact-angle and a smooth lustrous surface can be deposited using surface fluorination. The most effective method is to allow Al to react with graphite or graphite fluoride in the presence of F_2-gas (0.1–1 bar) at high temperature (450–600°C). The film, which is 3 μm thick, contains large amounts of fluorine and aluminum and only small content of carbon. The contact angle of water on the film is 125° and the resistance is greater than 4×10^{10} Ω cm^{-1}. In addition these films exhibit a good inertness with high resistance to acidic and alkaline corrosions and high thermal stability [89,113]. It can be added that in reactive ion etching reactions involving a mixture of fluorocarbon gases, a passivation layer (AlF_x) containing only small amount of carbon is also formed onto the reactor (Al) surface [114].

14.3.2.2 Adhesive properties of aluminum surfaces

One of the main inconvenience for the use of composite materials based on an Al matrix remains the difficulty to obtain interfaces of high quality because of the presence of an alumina layer which hinders the adhesion during the casting. Surface treatments by PEF or by low-temperature F_2-gas fluorination lead to the formation of a very reactive aluminum fluoride film onto the metal [89,115]. Once fluorinated, the Al-based reinforcements can be set inside a mould in such a way that molten Al comes into contact with their surface. After casting, a noticeable increase of the tensile strength of the specimens reinforced by PEF-treated insets is observed, the rupture threshold being largely higher than that of bulky Al pieces [113]

14.3.2.3 Intermetallic compounds for hydrogen storage

A number of intermetallic compounds have been reported to absorb large amounts of hydrogen. However, large scale commercial applications of metal hydrides for the separation and purification of hydrogen have not been yet fully achieved because of the high sensitivity of the metal surface to gaseous impurities present in hydrogen, and also because of possible pyrophobicity in air.

The surface properties of such materials can be highly improved by a treatment in aqueous HF solutions. This processing has been applied to various series of alloys

and intermetallic compounds, such as La $Ni_{4.7}Al_{0.3}$ and Mg_2Ni, by S. Suda et al. [116]. The initial pH of the solution is set close to 5; during the experiment, a continuous consumption of F^- ions of the solution is caused by the formation of a solid fluoride film on the metal surface. Meanwhile the pH increases with several reaction steps that result from the decomposition of La oxide and hydroxide present on the surface and at the grain boundaries, that finally leads to the formation of a fluoride film rich in La, with the dissolution of Ni^{2+} ions in the solution. The complete reaction thus corresponds to the formation of a fluorinated layer, a few nm thick, and containing numerous catalytic Ni clusters instead of the originally oxide/hydroxide-contaminated material.

F-treated intermetallics exhibit extremely high reactivity and selectivity to H_2, even in CO and CO_2 atmospheres. The treatment behaves as a curing effect of the external surface and creates a fluoride-rich layer with a Ni-enriched subsuperficial layer. The hydriding behavior is increased by the presence of microcracks running through the external layer: the initial activation process is enhanced, even for Mg-based alloys. In addition, a protective effect is observed since the samples can be safely stored in air for long time without degradation or surface reactivity [116].

14.3.2.4 Protection of diamond film coatings

The surface properties of many systems can be significantly improved by the use of coating exhibiting specific characteristics. Because of their outstanding properties, diamond films are involved in the coating of many products, such as cutting tools, optical items (disks, lenses, windows), biological implants.

It appeared decisive to modify chemically the outer surface of the diamond film itself, in order to create new surface properties. In particular when diamond is exposed to relatively high temperature or to varied stresses, its surface can easily transform to graphite in an irreversible process. Because of its reactivity, fluorine may act as a modifier which could improve some surface properties of diamond: lubricant properties, stability under oxidising conditions. In this scope, molecular F_2, atomic F, or XeF_2 have been proposed as fluorinating media [117]. This improvement is particularly important since diamond can be grown at relatively low temperatures by CVD techniques. For instance, the exposition of a clean (111) surface of diamond to XeF_2-gas leads to the dissociative chemisorption of fluorine, releasing Xe into the ambiant. The clean surface had been prepared by heating the crystal in ultravacuum above the hydrogen desorption temperature. Around 80% of the surface of diamond is covered by C—F bonds as shown by the C1s photoemission spectra [118].

Similar results are obtained with microwave discharged (2450 MHz) SF_6 vapor at $P = 1$ mTorr during reaction durations ranging from a few min to several hours. After 20 min exposure, an average thickness of about 2 monolayers of diamond has been converted to fluorocarbon of CF formulation, in which CF_2 and CF_3 groups are also present [119]. Direct fluorination by F_2-gas allows to replace hydrogen chemisorbed on the surface by fluorine at very low temperature, even at $-10°C$, whereas in the case of surface oxidised diamond, a complete replacement

of oxygen by fluorine is obtained for fluorination temperatures higher than 500°C [120].

14.3.2.5 PECVD of fluorinated diamond-like carbon films (hydrogenated amorphous films)

Interlayer dielectrics with a low dielectric constant are required to reduce the parasitic capacitance in ultralarge scale integration circuits. Although fluoropolymers such as PTFE have been for long time the lowest dielectric material, their low adhesive strength, low thermal stability and difficulty of manufacturing have limited their development in microelectronics. These films of fluorinated amorphous carbon (a-C:F) have been prepared for a similar purpose in a PECVD equipment using CF_4—CH_4 rf plasmas in 100–200 mTorr pressure at 50°C. The films that were grown at a 10 nm min^{-1} rate were deposited on SiO_2/(100) Si and (100) p^+ Si wafers previously covered by a thin film of hydrogenated amorphous carbon. Films with a dielectric constant as low as 2.1 were obtained [121]. In such systems, the leakage current is reduced to 10^{-8} A cm^{-2} by the use of (a-C:F) film. Since the electrical conduction in amorphous carbon takes place by hopping mechanism between localised states distributed in the mobility gap, the observed reduction of the leakage current can be assigned to the reduction of localised states by fluorination. It can be pointed out the decisive role of fluorinated DLC films for wear-resistant protective coatings [122,123]. The micro-tribological characteristics of Si-containing hard carbon films deposited on Si substrate are improved by CF_4 treatments: surface energy is reduced and so the micro-wear at an atomic scale [133,134].

14.3.2.6 Modification of wettability of materials

The modification of wettability of materials surfaces is in most cases a parameter of primary importance. Depending on the choice of application, the coating may exhibit either a high water repellency associated with lubricative and mold resealing properties or a high wettability, as in the case of carbon fibers to increase for instance their adhesion with the matrix in composites. We have seen in Sec. 14.3.1.1 that fluorination treatments of carbon materials using low-pressure plasmas or F_2-gas generally lead to an enhancement of water repellency. This effect is due to the decrease of surface free energy that corresponds to the low polarisability of the covalent C—F bond, formed at the surface. The deposition of films formed of a metal/perfluoro compound composite on various types of substrates also leads to super repellent properties [124]. The metal is generally Ni and the perfluoro compound, such as PTFE or graphite fluoride $(CF)_n$ should have been previously treated under F_2-gas. This fluorination treatment is required to increase the number of CF_3 groups at the surface of the particles. The very high contact-angle of water droplets on Ni/F_2-treated PTFE ($\theta \sim 170°$) is much higher than that observed on a PTFE plate ($\theta = 110°$), as shown in Fig. 27.

These metal/F_2-treated PTFE composite films, with metals such as Ni, Au, Sn, Cr can also be prepared by electrodeposition in an electrolyte solution in which PTFE micrometric particles are suspended by using a cationic surfactant. In addition to their very high contact angle ($130 \leq \theta(°) \leq 155$), the films show good corrosion

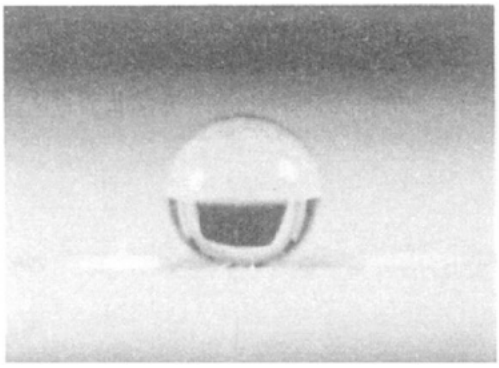

Fig. 27. Water droplet on an Ni/F_2-treated PTFE composite substrate, with contact angle of 173° (with courtesy of Y.B. Chong and N. Watanabe, Kyoto, (1991)).

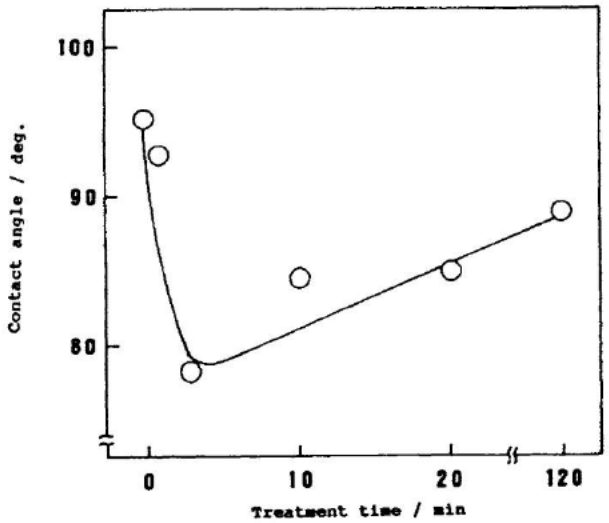

Fig. 28. Dependence of the contact angle upon the F_2-gas fluorination time (reproduced with permission from J. Fluorine Chem., 57 (1992) 169 [126]).

resistivity and thermal stability at 325°C in air [125]. On the other hand, improvement of wettability of various carbon surfaces fibers or powders has been achieved with very short fluorination times by F_2-gas. The minimum value of contact angle observed for water droplets ($\theta = 78°$) is obtained for 3 min fluorination at 25°C under 10 Torr F_2-gas pressure, as shown in Fig. 28. The increase of wettability can be correlated with the increase of surface polar components and of oxygen content (C/O/F contents (%): 77.3/12.2/10.5) [126].

14.3.2.7 Electrochemical properties of cathode materials

$LiMO_2$, with M = Co, Fe, Ni, are currently used as cathode in Li-ion secondary batteries. The electrochemical characteristics of these materials can be modified by surface fluorination. The fluorinating gases can be either NF_3 or ClF_3 in the following conditions: $p = 10$ mTorr; room temperature $< T < 200°C$; reaction duration = 1 h. After the treatment with ClF_3, the peaks of the cyclic voltammograms of $LiCoO_2$ become broad and the tailing below 3.5 V during the cathodic sweep disappears. The average charge/discharge potential of ClF_3-treated $LiCoO_2$ is more anodic than those of untreated and NF_3-treated samples [127].

14.3.2.8 Conversion of cuprate oxide thin films into superconductors

Pulsed laser ablation has been developed in many fields for the fabrication of thin films of oxide materials, in particular high T_C cuprate superconductors. In these materials, the increase of the carrier concentration can be obtained in many cases by chemical doping (cationic or anionic), in order to induce superconductivity.

In La_2CuO_4 thin films, the anionic modification of the carrier concentration has been achieved by annealing the films in an oxidising (F_2-gas) atmosphere [128]. The films were prepared on (100) $SrTiO_3$ substrates by pulsed laser ablation from the oxide targets. Fluorine doping of La_2CuO_4 was then carried out by a treatment at 100–200°C under 10% F_2 in N_2. It is possible to control anionically the carrier concentration in the deposited thin films, in order to optimise the conditions, resulting in films with $T_C \sim 36$ K. From hysteresis cycles, critical current density (J_C) of 10^6 A cm^{-2} are observed at 10 K under zero field [128]. Thin films of $YBa_2Cu_3O_{7-\delta}$ prepared by the same method have been transformed into superconductors by NF_3 treatments [129,130]. The final T_C value, which can be as high as 89 K, depends on the initial oxygen deficiency. In addition, this fluorination treatment acts as a protection against moist air.

14.3.2.9 Fluorinated silicon dioxide films

Speed in Ultra Large Scale Integrated devices can be increased by reducing the capacitance of the interlayer insulators. Since SiO_2 is the material most used for such components, the replacement of oxygen by fluorine has attraced much interest this last decade. PECVD is generally used to elaborate these layers and it involves fluorinated gases such as CF_4, SiF_4, CCl_2F_2, C_2F_6 [135,136].

14.4 Concluding remarks

Surface fluorination in various fluorinated media are currently used nowadays as processes that allow the modifications of many classes of materials, such as metals, intermetallics, semiconductors, carbons, superconductors, oxide ceramics. The above selected examples have illustrated some physical properties that can be drastically modified, including conduction, adhesion, passivation, superconductivity, hydrophobicity/wettability.

Acknowledgments

The authors would like to thank G. Turban and Mrs M.C. Peignon for comments, suggestions and encouragements. In Part II several examples (carbon materials and superconducting ceramics) have been taken from work carried out at ICMCB by F. Moguet and C. Magro during the course of their Doctorate theses. Messrs T. Shirasaki, L. Lozano (ICMCB-Bordeaux), C. Guimon (LPCM-Pau), G. Nansé, E. Papirer (ICSI-Mulhouse) are acknowledged for fruitful discussions and collaboration.

List of symbols of Part I

A^* : radiative activated species
a_0 : Bohr radius,

$$a_0 = \frac{4 \cdot \pi \cdot \varepsilon_0 \cdot \hbar}{e^2 \cdot m_e} = 5.2918 \times 10^{-11}\ \mathrm{m}$$

c : velocity (m s^{-1}), $\langle c \rangle$ average velocity

e : electron charge (C)

E : energy (J), $\langle E \rangle$ average energy
ER : etch rate (m s^{-1}) or (atom s^{-1})

f : distribution function,

$$\mathrm{MBD}(E_e) = \frac{2}{\sqrt{\pi}} \cdot \frac{1}{(k \cdot T_e)^{\frac{3}{2}}} \cdot \sqrt{E_e} \cdot \exp\left[-\frac{E_e}{k \cdot T_e}\right]$$

or,

$$f(c_e) = 4 \cdot \pi \cdot \left(\frac{m_e}{2 \cdot \pi \cdot k \cdot T_e}\right)^{\frac{3}{2}} \cdot c^2 \cdot \exp\left[-\frac{m_e \cdot c_e^2}{2 \cdot k \cdot T_e}\right]$$

I : emission intensity (au)
K : rate constant

k : Boltzmann constant
M : material

α_P : polarisability
ε_0 : permittivity of vacuum

λ : length (m), wavelength, mean free path, or Debye mean free path:

$$\lambda_{A/B} = \frac{\langle c_A \rangle}{\langle v_{A/B} \rangle}$$

σ : cross section (m^2), hard sphere: $\sigma_{A/B} = \pi \cdot (r_A + r_B)^2$,
polarisation scattering:

$$\sigma_{A/B} = \sqrt{\frac{\pi \cdot e^2}{\varepsilon_0} \cdot \alpha_p \cdot \frac{m_A + m_B}{m_A \cdot m_B}} \cdot \frac{1}{c_{A/B}}$$

Φ: flux density (m^{-2} s^{-1})
υ: frequency (Hz), radiation, plasma, or collision,
collision:
$\langle v_{A/B} \rangle = \int_e n_B \cdot \sigma_{A/B} \cdot c_{A/B} \cdot f(c_{A/B}) \cdot \mathrm{d}c_{A/B}$
ω : angular frequency (Hz)

Signification of subscripts

a : adsorption
A/B : process between particle A (incident) and B (target)
ces : chemical enhanced sputtering
d : desorption (thermal)

m : mass (kg)
n : density (m^{-3}), n': density at the vicinity of a surface
P : pressure (Pa)
r : particle radius in the hard sphere approximation (m)
S : surface (m^2)
T : temperature (K)
V : potential (V)
Y : sputtering yield

e : electron
i : ion

iar : ion assisted reaction
n : neutral particle

p : heavy particle (ion or neutral)
r : reaction (thermal)
s : sputtering
th : threshold

References

[1] A. Grill, Cold Plasma in Materials Fabrication, IEEE Press, NY, 1993.
[2] D.M. Manos, D.L. Flamm, Plasma Etching an introduction, Plasma-Materials Interaction Series, Academic Press, San Diego, 1989.
[3] O. Auciello, D.L. Flamm, Plasma Diagnostics, Plasma-Materials Interaction Series, Academic Press, San Diego, 1989.
[4] B. Chapman, Glow Discharge Processes, J. Wiley & Sons NY, 1980.
[5] M.A. Lieberman, A.J. Lichtenberg, Principles of Plasma Discharges and Material Processing, J. Wiley & Sons NY, 1994.
[6] I. Langmuir, Proc. Nat. Acad. Sci. U.S., 14 (1928) 627.
[7] H. Winters, Phys. Rev., A 25 (1982) 1420.
[8] A.D. Kuypers, H.J. Hopman, J. Appl. Phys., 67 (1990) 1229.
[9] P. Benoit-Cattin, L-C. Bernard, J. Appl. Phys., 39 (1968) 5723.
[10] J. Liu, L. Huppert, H.H Sawin, J. Appl. Phys., 68 (1990) 3916.
[11] A. Manenschijn, G.C.A.M. Janssen, E. van der Drift, S. Radelaar, J. Appl. Phys., 69 (1990) 1253.
[12] A. Picard, G. Turban, B. Grolleau, J. Phys. D: Appl. Phys., 19 (1986) 991.
[13] W.H. Beattie, Applied Spectroscopy, 29 (1975) 334.
[14] G. Turban, B. Grolleau, P. Launay, P. Briaud, Rev. Phys. Appl., 20 (1985) 609.
[15] E.A. Truesdale, G. Smolinsky, J. Appl. Phys., 50 (1979) 6594.
[16] H. Sugai, H. Toyoda, J. Vac. Sci. Technol., A 10 (1992) 1193.
[17] A. Tserepi, W. Schwarzenbach, J. Derouard, N. Sadeghi, J. Vac. Sci. Technol., A 15 (1997) 3120.
[18] W.W. Stoffels, E. Stoffels, K. Tachibana, J. Vac. Sci. Technol., A 16 (1998) 87.
[19] L.J. Overzet, J.H. Beberman, J.T. Verdeyen, J. Appl. Phys., 66 (1989) 1622.
[20] E. Stoffels, W.W Stoffels, D. Vender, G.M.W. Kroesen, F.J. de Hoog, J. Vac. Sci. Technol., A 13 (1995) 2051.
[21] M-C. Peignon, Ch. Cardinaud, G. Turban, J. Electrochem. Soc., 140 (1993) 505.
[22] J.W. Coburn, M. Chen, J. Appl. Phys., 51 (1980) 3134.
[23] R. d'Agostino, F. Cramarossa, S. de Benedictis, G. Ferraro, J. Appl. Phys., 52 (1981) 1259.
[24] V.M. Donnelly, D.L. Flamm, W.C. Dautremont-Smith, D.J. Ferder, J. Appl. Phys., 55 (1984) 242.
[25] M. Haverlag, W.W. Stoffels, E. Stoffels, G.M.W. Kroesen, F.J. de Hoog, J. Vac. Sci. Technol., A 14 (1996) 384.

[26] M. Haverlag, W.W. Stoffels, E. Stoffels, G.M.W. Kroesen, F.J. de Hoog, J. Vac. Sci. Technol., A 14 (1996) 380.
[27] K. Miyata, M. Hori, T. Goto, J. Vac. Sci. Technol., A 15 (1997) 568.
[28] B.K. McMillin, M.R. Zacharian, J. Vac. Sci. Technol., A 15 (1997) 230.
[29] C. Suzuki, K. Sasaki, K. Kadota, J. Vac. Sci. Technol., A 16 (1998) 2222.
[30] K. Miyata, M. Hori, T. Goto, J. Vac. Sci. Technol., A 14 (1996) 2343.
[31] J-P. Booth, G. Hancock, N.D. Perry, M.J. Toogood, J. Appl. Phys., 66 (1989) 5251.
[32] K.E. Greenberg, P.J. Hargis Jr, J. Appl. Phys., 68 (1990) 505.
[33] G. Cunge, P. Chabert, J-P. Booth, Plasma Sources Sci. Technol., 6 (1997) 349.
[34] V.A. Godyak, R.B. Piejak, B.M. Alexandrovich, Plasma Sources Sci. Technol., 1 (1992) 36.
[35] N Hershkowitz, In: Plasma Diagnostics: Discharge Parameters and Chemistry, O. Auciello, D.L. Flamm (Eds.), Plasma-Materials Interaction Series, Academic Press, San Diego, 1989, p. 113.
[36] M.B. Hopkins, J. Res. Nat. Inst. Stand. Technol., 100 (1995) 415.
[37] M-C. Peignon, Ch. Cardinaud, G. Turban, J. Appl. Phys., 70 (1991) 3314.
[38] D.C. Marra, E.S. Aydil, J. Vac. Sci. Technol., A 15 (1997) 2508.
[39] G.S. Oehrlein, J. Vac. Sci. Technol., A 11 (1993) 34.
[40] T. Shirafuji, W.W. Stoffels, H. Moriguchi, K. Tachibana, J. Vac. Sci. Technol., A 15 (1997) 209.
[41] G.M.W. Kroesen, H-J Lee, H. Moriguchi, H. Motomura, T. Shirafuji, K. Tachibana, J. Vac. Sci. Technol., A 16 (1998) 225.
[42] S. Vallon, O. Joubert, L. Vallier, F. Ferrieu, B. Drevillon, N. Blayo, J. Vac. Sci. Technol., A 15 (1997) 865.
[43] M.J.M. Vugts, M.F.A. Eurlings, L.J.F. Hermans, H.G.W. Beijerinck, J. Vac. Sci. Technol., A 14 (1996) 2780.
[44] R. Pétri, P. Brault, O. Vatel, D. Henry, E. André, P. Dumas, F. Salvan, J. Appl. Phys., 75 (1994) 1.
[45] T. Chevolleau. Doctorate Thesis, Univ. Nantes-ISITEM, Nantes, France, 1998.
[46] R.N. Compton, L.G. Christophorou, G.S. Hurst, P.W. Reinhardt, J. Chem. Phys., 45 (1966) 4634.
[47] L.G. Christophorou, J.K. Olthoff, V.V.S. Rao, J. Phys. Chem. Ref. Data, 25 (1996) 1341.
[48] A.V.P. Phelps, J. Appl. Phys., 64 (1988) 4269.
[49] H.G. Lergon, M. Venugopalan, K.G. Müller, Plasma Chem. Plasma Process., 4 (1984) 107.
[50] K.R. Ryan, I.C. Plumb, Plasma Chem. Plasma Process., 6 (1986) 231.
[51] Y. Hikosaka, H. Toyoda, H. Sugai, Jpn. J. Appl. Phys. Part 2, 32 (1993) 353.
[52] N.V. Mantzaris, E. Gogolides, A.G. Boudouvis, Plasma Chem. Plasma Process., 16 (1996) 301.
[53] I.C. Plumb, K.R. Ryan, Plasma Chem. Plasma Process., 6 (1986) 205.
[54] J.C. Martz, D.W. Hess, W.E. Anderson, Plasma Chem. Plasma Process., 10 (1990) 261.
[55] A. Campo, Ch. Cardinaud, G. Turban, Plasma Sources Sci. Technol., 4 (1995) 398.
[56] J-P. Booth, G. Hancock, N.D. Perry, Appl. Phys. Lett., 50 (1987) 318.
[57] J-P. Booth, G. Hancock, N.D. Perry, D.C.W. Blaikeley, J.A. Cairn, R. Smailes, Mat. Res. Soc. Symp. Proc. 98 (1987) 135.
[58] K.R. Ryan, I.C. Plumb, Plasma Chem. Plasma Process., 10 (1990) 207.
[59] S.P. Venkatesan, I. Trachtenberg, T.F. Edgar, J. Electrochem. Soc., 137 (1990) 2280.
[60] R.A.H. Heinecke, Solid-State Electron., 18 (1975) 1146.

[61] J.W. Coburn, J. Appl. Phys., 50 (1979) 5210.
[62] H-H. Doh, J-H. Kim, K-W. Whang, S-H. Lee, J. Vac. Sci. Technol., A 14 (1996) 1088.
[63] G.S. Oehrlein, H.L. Williams, J. Appl. Phys., 62 (1987) 662.
[64] G.S. Oehrlein, Mat. Res. Soc. Symp. Proc., 98 (1987) 229.
[65] A. Campo, Ch. Cardinaud, G. Turban, J. Vac. Sci. Technol., B 13 (1995) 235.
[66] J.W. Coburn, H.F. Winters, J. Appl. Phys., 50 (1979) 3189.
[67] D.L. Flamm, V.M. Donnelly, J.A. Mucha, J. Appl. Phys., 52 (1981) 3633.
[68] P.C. Zalm, J. Appl. Phys., 54 (1983) 2660.
[69] J.L. Mauer, J.S. Logan, L.B. Zielinski, G.C. Schwartz, J. Vac. Sci. Technol., 15 (1978) 1734.
[70] T. Chevolleau, P-Y. Tessier, Ch. Cardinaud, G. Turban, J. Vac. Sci. Technol., A 15 (1997) 2661.
[71] M.E. Barone, D.B. Graves, J. Appl. Phys., 77 (1995) 1263.
[72] M.E. Barone, D.B. Graves, J. Appl. Phys., 78 (1995) 6604.
[73] P. Alnot, J. Olivier, F. Wyczisk, J. Electron Spectrosc. Relat. Phenom., 43 (1987) 263.
[74] A. Campo, Ch. Cardinaud, G. Turban, C. Dubon-Chevallier, V. Amarger, J. Etrillard, J. Vac. Sci. Technol., A 11 (1993) 2536.
[75] J.W. Butterbaugh, D.C. Gray, H.H. Sawin, J. Vac. Sci. Technol., B 9 (1991) 1461.
[76] D.C. Gray, I. Tepermeister, H.H. Sawin, J. Vac. Sci. Technol., B 11 (1993) 1243.
[77] M.J.M. Vugts, L.J.F. Hermans, H.G.W. Beijerinck, J. Vac. Sci. Technol., A 14 (1996) 2138.
[78] J. Ding, J-S. Jenq, G-H. Kim, H.L. Maynard, J.S. Hamers, N. Hershkowitz, J.W. Taylor, J. Vac. Sci. Technol., A 11 (1993) 1283.
[79] D. Dane, T.D. Mantei, Appl. Phys. Lett., 65 (1994) 478.
[80] M-C. Peignon, G. Turban, C. Charles, R.W. Boswell, Surf. Coating Technol., 97 (1997) 465.
[81] Y. Feurprier, Ch. Cardinaud, B. Grolleau, G. Turban, J. Vac. Sci. Technol., A 16 (1998) 1552.
[82] N.R. Rueger, J.J. Beulens, M. Schaepkens, M.F. Doemling, J.M. Mirza, T.E.F.M. Standaert, G.S. Oehrlein, J. Vac. Sci. Technol., A 15 (1997) 1881.
[83] Ch. Cardinaud, G. Turban, Appl. Surf. Sci., 45 (1990) 109.
[84] C.J. Mogab, A.C. Adams, D.L. Flamm, J. Appl. Phys., 49 (1978) 3796.
[85] A. Picard, G. Turban, Plasma Chem. Plasma Process., 5 (1985) 333.
[86] M-C. Peignon, Ch. Cardinaud, G. Turban, J. Appl. Phys., 70 (1991) 3314.
[87] M-C. Peignon. Doctorate Thesis, Univ. Nantes-ISITEM, Nantes, France, 1993.
[88] U. Kortshagen, A. Shivarova, E. Tatrova, D. Zamfirov, J. Phys. D: Appl. Phys., 26 (1994) 301.
[89] N. Watanabe, T. Nakajima, H. Touhara, Graphite Fluorides, Elsevier, Amsterdam, 1988.
[90] R.J. Lagow, L.A. Shimp, D.K. Lam, R.F. Baddour, Inorg. Chem., 11 (1972) 2568.
[91] G.D. Merfeld, M.A. Petrich, J. Vac. Sci. Technol., A12 (1994) 365
[92] K. Kotera, H. Tanaka, M. Uchida, T. Hirao, N. Iwamoto, J. Japan Inst. Metals, 60 (1996) 595.
[93] S. Okazaki, M. Kogoma, S. Kanazawa, T. Moriwaki, Proc. Jap. Symp. Plasma Chem., 1 (1988) 251.
[94] I.H. Loh, R.E. Cohen, R.F. Baddour, J. Mater. Sci., 22 (1987) 2937.
[95] T. Nakajima, N. Watanabe, Graphite Fluorides and Carbon-Fluorine Compounds, CRC Press, Boca Raton, 1991.
[96] A. Tressaud, Mol. Cryst. Liq. Cryst., 244 (1994) 13.

[97] T. Mallouk, N. Bartlett, J. Chem. Soc. Chem. Commun., 103 (1983).
[98] A. Tressaud, C. Guimon, V. Gupta, F. Moguet, Mat. Sc. Engin., B30 (1995) 61.
[99] F. Moguet, Doctorate Thesis, Univ. Bordeaux I, (1996).
[100] A. Tressaud, V. Gupta, L. Piraux, L. Lozano, E. Marquestaut, S. Flandrois, A. Marchand, O.P. Bahl, Carbon, 32 (1994) 1485.
[101] G. Nansé, E. Papirer, P. Fioux, F. Moguet, A. Tressaud, Carbon, 35 (1997) 175.
[102] G. Nansé, E. Papirer, P. Fioux, F. Moguet, A. Tressaud, Carbon, 35 (1997) 371.
[103] G. Nansé, E. Papirer, P. Fioux, F. Moguet, A. Tressaud, Carbon, 35 (1997) 515.
[104] J.M. Dance, A. Tressaud, B. Chevalier, J. Darriet, J. Etourneau, Solid State Ionics, 32/33 1989 p 1188.
[105] B. Lépine, Doctorate Thesis, Univ. Bordeaux I, 1990.
[106] J.M. Heintz, C. Magro, A. Tressaud, P. Dordor, J.P. Bonnet, J. Less-Comm. Metals, 164–165 (1990) 1377.
[107] C. Magro, Doctorate Thesis, Univ. Bordeaux I, 1992.
[108] C. Magro, A. Tressaud, L. Lozano, J. Etourneau, N. Hudakova, C. Cardinaud, G. Turban, J. Mat. Sci., 29 (1994) 4225; ibid. 4260.
[109] W. Herzog, M. Schwarz, H. Sixl, R. Hoppe, Z. Phys., B71 (1988) 19.
[110] S. Myhra, J.C. Rivière, A.M. Stewart, P.C. Healy, Z. Phys., B72 (1988) 413.
[111] R.P. Vasquez, M.C. Foote, B.D. Hunt, J. Appl. Phys., 66 (1989) 4866.
[112] A. Tressaud, K. Amine, J.P. Chaminade, J. Etourneau, Tran Minh-Duc, A. Sartre, J. Appl. Phys., 68 (1990) 248.
[113] C. Briant, J.C. Da Rugna, A. Tressaud, F. Girot, French Patent no. 9501786 (1995).
[114] J.F. Daviet, L. Peccoud, P. Lassagne, A. Ermolieff, S. Marthon, F. Pierre, Le Vide, Les Couches Minces, Suppl. No 256, Société Française du Vide, Paris, (1991) 365.
[115] H. Yamada, T. Nakajima, N. Watanabe, Angew. Chem. Int. Ed., 21 (1982) 378.
[116] F.J. Lin, S. Suda, J. Alloys Compounds, 231 (1995) 742 (and several other contributions in the same issue).
[117] D.E. Patterson, R.H. Hauge, J.L. Margrave, Mat. Res. Soc. Symp. Proc., 140 (1989) 351.
[118] J.F. Morar, F.J. Himpsel, G. Hollinger, J.L. Jordan, G. Hughes, F.R. McFeely, Phys. Rev., B33 (1986) 1340; ibid. 1346.
[119] P. Cadman, J.D. Scott, J.M. Thomas, J. Chem. Soc., Chem. Commun., (1975) 654.
[120] T. Ando, K. Yamamoto, M. Kano, Y. Sato, Y. Takamatsu, S. Kawasaki, F. Okino, H. Touhara, J. Chem. Soc., Faraday Trans., 91 (1995) 3209.
[121] K. Endo, T. Tatsumi, J. Appl. Phys., 78 (1995) 1370.
[122] J. Seth, S.V. Babu, Thin Solid Films, 230 (1993) 90.
[123] A. Grill, V.V. Patel, U. S. Patent 5, 674, 638, (1997).
[124] Y.B. Chong, N. Watanabe, Proc. 13th Intern. Symp. Fluorine Chem., Contribution A-43, Bochum, Germany, 1991.
[125] H. Kiyokawa, T. Kiyokawa, R. Ikeda, S. Yonezawa, Y.B. Chong, M. Takashima, Proc. 3rd Conf. on High Performance Coating Materials: Fluorine in Coatings II, (Contribution 12), Munich, Germany, 1997.
[126] Y.B. Chong, H. Ohara, J. Fluorine Chem., 57 (1992) 169.
[127] S. Yonezawa, A. Hirano, T. Kimura, M. Takashima, Proc. 12th Europ. Symp. Fluorine Chem., Contribution PI-83, Berlin, Germany, 1998.
[128] S.T. Lees, I. Gameson, M.O. Jones, P.P. Edwards, C. Greaves, F. Wellhofer, P. Woodall, I. Langford, M. Slaski, Physica, C270 (1996) 305.
[129] O. Peña, M. Mokhtari, C. Perrin, C. Thivet, M. Guilloux-Viry, A. Perrin, M. Sergent, Physica, C206 (1993) 6.

[130] P. Massiot, Doctorate Thesis, Univ. Rennes I, 1998.
[131] M.R. Wertheimer, L. Martinu and E.M. Liston, Handbook of Thin Film Process Technology, Chapter E3.0, IOP Publ., Bristol, 1996.
[132] Y. Hattori, Y. Watanabe, S. Kawasaki, F. Okino, B.K. Pradhan, T. Kyotani, A. Tomita, H. Touhara, Carbon, 37 (1999) 1033.
[133] S. Miyake, R. Kaneko, Y. Kikuya, I. Sugimoto, J. Tribology, Trans. ASME, 113 (1991) 384.
[134] C. Donnet, Surf. Coatings Techn. 100–101 (1998) 180.
[135] M. C. Paul, R. Sen, T. Bandyopadhyay, J. Mater. Sci. 32 (1997) 3511.
[136] S. Hasegawa, T. Tsukaoka, T. Inokuma, Y. Kurata, J. Non-Cryst. Solids 240 (1998) 154.